Investigation Into the Galloping Characteristics of Multispan Iced Covered Conductors

JIA-YAN ZHENG[1,2], QI-HANG SHEN[ID][1], AND XIAO-HUI LIU[1,2]
[1]School of Civil Engineering, Chongqing Jiaotong University, Chongqing 4400074, China
[2]State Key Laboratory of Bridge and Tunnel Engineering in Mountain Areas, Chongqing Jiaotong University, Chongqing 400074, China

Corresponding author: Qi-Hang Shen (545402808@qq.com)

ABSTRACT A full multispan two-degree-of-freedom (2-DOF) iced covered transmission line model is presented. Taking multispan conductors as the research object, based on the Hamiltonian principle, a non-linear galloping model of multispan conductors considering the influence of insulator strings is established, and its galloping equation is derived. Based on the theoretical formula, the modes and frequencies in-plane and out-of-plane of the multispan conductor plane were obtained. After the partial differential equation was transformed into an ordinary differential equation by the Galerkin discrete method, the multiple scale method was used to solve the dynamic response of the multispan conductors. Through numerical calculations, this study is the first to systematically analyze the effects of parameters such as span number, span length, and tension on the in-plane and out-of-plane motion characteristics of multi-span conductors from a theoretical perspective. The research results in this paper have certain reference value for preventing multispan conductor galloping and interphase flashover.

INDEX TERMS Iced covered transmission lines, mode, multispan, natural frequency, nonlinear galloping.

I. INTRODUCTION

The galloping of the ice covered conductors will cause hardware wear and damage transmission lines, seriously hindering the normal operation of the line and bringing huge losses to the national economy [1]. The investigation of ice covered conductor galloping has important practical engineering value for the development of galloping prevention and galloping suppression technology.

According to different types of galloping phenomena, Den Hartog proposed a vertical galloping mechanism [2], Nigol proposed a torsional galloping mechanism [3], [4], and Yu proposed an eccentric inertial coupling mechanism [5], [6] on the basis of the former. These three galloping mechanisms can explain the causes of galloping well, so it is generally accepted. On this basis, scholars from all over the world have put forward more galloping models of iced covered conductors. The main research methods include experiments, theoretical derivations and finite element methods. The aerodynamic characteristics of conductors are the premise of research on galloping [7]. The wind tunnel experiment

conducted in the literature [8] considered the aerodynamic parameters of single conductors at different wind speeds. In the wind tunnel experiment conducted in reference [9], the influence of turbulence was added to measure the aerodynamic parameters of single span conductors with different ice-covered shapes. In the wind tunnel experiment described in the literature [10], the aerodynamic coefficients of each subconductor of the four-split conductors were measured. The study found that the wake effect had a great influence on the aerodynamic characteristics. The conductor mode and frequency are the keys to the theoretical study of ice covered conductor galloping. Reference [11] proposed the theory of linear free vibration of suspension cable with a small sag, and the normal symmetric mode of cable depends on a dimensionless parameter. Reference [12] extends the theory of suspension cables to stay cables. Reference [13] revises the formula of mode and frequency of stay cables proposed by Irvine, considering the influence of cable tilt angle on mode and frequency. According to the observation of extensive field data, the galloping of the ice-covered conductors is actually the galloping of the conductors in the tension section, so it is of great significance to study the galloping characteristics of the multispan conductors. With the maturity of computer

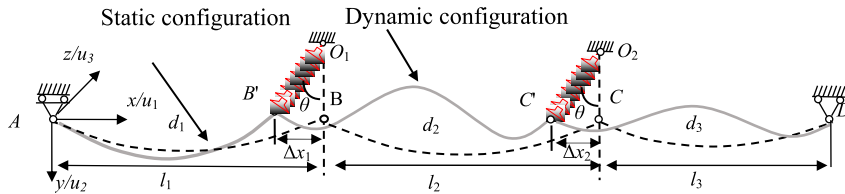The associate editor coordinating the review of this manuscript and approving it for publication was Shihong Ding[ID].

FIGURE 1. Multispan conductor model.

software, the finite element method has become an effective method to study the galloping characteristics of multispan conductors. This is because theoretical studies have focused on single-span conductors.

However, the existing single-span conductor theory fails to consider the influence of the interaction between insulator strings and conductors, so the galloping characteristics of multispan conductors cannot be studied. In references [14], [15], the finite element model of 3-DOF multispan conductors was established by using a three-node isoparammetric cable element. The study found that the amplitude of three-span conductors was much greater than that of single-span conductors, so the interaction between conductors could not be ignored.

A review of the research of the above scholars shows that few scholars have adopted the theoretical derivation method to study the galloping of multispan conductors at present. Reference [16] carried out a simple theoretical study on parallel length multispan conductors and believed that only the mode and frequency of the conductors could be obtained before the theoretical study on multispan conductor galloping could be carried out. Reference [17] established two independent coordinate systems to focus on the frequency and mode of the two-span conductors but ignored the axial motion of the conductors, and the dynamic tension changes caused by galloping cannot be ignored. Reference [18] considered the oscillating problem of insulators and the axial movement of multispan conductors and proposed the theoretical formula for calculating the frequency and mode of multispan conductors for the first time.

Based on the literature [18], the galloping characteristics of multispan conductors are theoretically studied for the first time. A simplified galloping model of multispan conductors considering the influence of insulators is established, and its corresponding galloping equation is derived. The fourth-order Runge–Kutta method was used to solve the equation of galloping and compared with the finite element numerical simulation results and multiscale method of reference [14] to verify the rationality of the model. The calculation efficiency of the multispan transmission line galloping calculation method proposed in this paper is higher than that of the finite element method, and considering the nonlinear effects of transmission lines, it is more reasonable than methods found in the literature [14].

According to the calculation method proposed in this paper, the effects of parameters such as span number, span

length and tension on the galloping characteristics of multispan conductors are systematically analyzed for the first time from a theoretical point of view.

II. THE EQUATION OF MOTION OF ICED COVERED CONTINUOUS CONDUCTORS

A simplified mechanical model of iced covered conductors hinged at both ends without a height difference was established. The Cartesian coordinate system A-x-y-z was established with the left suspension point as the origin. The connection between the two hinged points was the x-axis, the positive direction of the y-axis was perpendicular to the downward x-axis, and the positive direction of the z-axis was perpendicular to the plane determined by x and y. The configuration of continuous span iced covered conductors can be divided into two types, namely, the static configuration under the natural state represented by the dotted line and the dynamic configuration under the wind load represented by the solid line, as shown in Fig. 1.

In Fig. 1, x, y, and z represent static displacement, and u_1, u_2, and u_3 represent dynamic displacement. The displacement in the y direction is vertical vibration, and the displacement in the z direction is horizontal vibration. li is the length of the i th span conductor, d_i is the sag of the i th span conductor, and the subscript i represents the i th span conductor.

To simplify the calculation, the following assumptions are made according to the actual situation of the transmission lines.

(1) Since the span is much larger than the diameter of the conductors, the bending stiffness and shear stiffness of the conductors are ignored. Since the axial displacement of the conductors is much smaller than the lateral displacement and the longitudinal vibration frequency is much higher than the transverse vibration frequency, the longitudinal displacement of the conductors is ignored.

(2) Assuming the sag ratio of any span conductor $d_i/l_i < 1/8$, the parabolic configuration can be used to describe the static configuration of the conductors. The static configuration y_i of any span conductor can be expressed as:

$$y_i = \frac{ql_i^2}{2H}\left(\frac{x}{l_i} - \left(\frac{x}{l_i}\right)^2\right) \tag{1}$$

In Equation (1), q is the weight of the conductors per unit length, and H is the static horizontal tension of the conductors. The initial horizontal tension of each spanning conductor is considered to be equal.

(3) Assuming that the ice is evenly distributed on the conductors, the influence of sectional eccentricity on galloping is not considered.

(4) The interaction between the tower and conductors is ignored.

The vibration equation of any span conductor can be obtained by the Hamiltonian variational principle:

$$\int_{t_0}^{t} \delta k^v \mathrm{d}t - \int_{t_0}^{t} \delta \prod \mathrm{d}t + \int_{t_0}^{t} \delta W \mathrm{d}t = 0 \quad (2)$$

In Equation (2), δ represents the first-order variation, k^v represents the kinetic energy, $\prod$ represents the potential energy, and W represents the work done by gravity, damping force and external force. The expressions of kinetic energy and potential energy are as follows:

$$\begin{cases} k^v = \int_0^{l_i} \frac{1}{2} m(\dot{u}_1^2 + \dot{u}_2^2 + \dot{u}_3^2) \mathrm{d}x \\ \prod = \int_0^{l_i} (H\varepsilon + \frac{1}{2}EA\varepsilon^2)\mathrm{d}x + \frac{1}{2}\int_0^{l_i} GI_P(\frac{\partial\theta}{\partial x})^2 \mathrm{d}x \end{cases} \quad (3)$$

In Equation (3), $(\cdot)$ represents the first-order derivative of time, m is the mass per unit length of conductors, EA is the tensile stiffness, GI_p is the torsional stiffness of conductor in the axial direction, θ is the torsional angle of conductor in the axial direction, ε is the total dynamic strain in the tension section, and its expression is as follows:

$$\varepsilon = \sum_{i=1}^{N} \frac{\int_0^{l_i} [\frac{\mathrm{d}y}{\mathrm{d}x}\frac{\partial u_2}{\partial x} + \frac{1}{2}(\frac{\partial u_2}{\partial x})^2 + \frac{1}{2}(\frac{\partial u_3}{\partial x})^2]\mathrm{d}x}{l_e} \quad (4)$$

In Equation (4), N is the number of spans, and l_e is the total length of the conductors in a tension section.

According to Equation (2), the nonlinear vibration equations of any span conductor of the multispan iced covered conductors are obtained:

$$\begin{cases} \frac{\partial}{\partial x}\{(\frac{\mathrm{d}y}{\mathrm{d}x} + \frac{\partial u_2}{\partial x})\frac{EA}{l_e} \\ (\sum_{i=1}^{N}\int_0^{l_i} \frac{\mathrm{d}y}{\mathrm{d}x}\frac{\partial u_2}{\partial x} + \frac{1}{2}((\frac{\partial u_2}{\partial x})^2 + (\frac{\partial u_3}{\partial x})^2)\mathrm{d}x) + H\frac{\partial u_2}{\partial x}\} \\ = m\ddot{u}_2 + \mu_2\dot{u}_2 - p_y \\ \frac{\partial}{\partial x}\{(\frac{\partial u_3}{\partial x})\frac{EA}{l_e} \\ (\sum_{i=1}^{N}(\int_0^{l_i} \frac{\mathrm{d}y}{\mathrm{d}x}\frac{\partial u_2}{\partial x} + \frac{1}{2}((\frac{\partial u_2}{\partial x})^2 + (\frac{\partial u_3}{\partial x})^2)\mathrm{d}x) + H\frac{\partial u_3}{\partial x}\} \\ = m\ddot{u}_3 + \mu_3\dot{u}_3 - p_z \\ 0 = J\ddot{\theta} - GI_P\frac{\partial^2\theta}{\partial x} + \mu_\theta\dot{\theta} - p_\theta \end{cases} \quad (5)$$

In Equation (5), μ_2 and μ_3 are damping coefficients of in-plane and out-of-plane, respectively, and p_y and p_z are aerodynamic forces of in-plane and out-of-plane, respectively.

The transverse and torsional displacements are represented through separate variables as follows: The product of $\psi_{yj(x)}$, $\psi_{zj(x)}$ and mode functions $q_{yj(t)}$, $q_{zj(t)}$ is separated by the mode

truncation method.

$$\begin{cases} u_2(x, t) = \sum_{j=1}^{\infty} \psi_{yj}(x)q_{yj}(t) \\ u_3(x, t) = \sum_{j=1}^{\infty} \psi_{zj}(x)q_{zj}(t) \\ u_\theta(x, t) = \sum_{j=1}^{\infty} \psi_{\theta j}(x)q_{\theta j}(t) \end{cases}$$

$$(6)$$

In Equation (6), the subscript j represents the mode order, $\psi_{yj(x)}$ is the in-plane modal function, $\psi_{zj(x)}$ is the out-plane modal function, $\psi_{\theta j(x)}$ is the tortional modal function, and $q_{yj(t)}$, $q_{zj(t)}$ and $q_{\theta j(t)}$ are the amplitudes of the discretizing modal functions.

The displacement function (6) is substituted into the nonlinear vibration Equation (5) of the iced covered conductors, and the nonlinear dynamic partial differential Equation (5) are transformed into nonlinear dynamic ordinary differential equations by the Galerkin method as follows:

$$\begin{cases} b_1\ddot{q}_{yj} + b_2\dot{q}_{yj} + b_3 q_{yj} + b_4 q_{yj}^2 + b_5 q_{zj}^2 + b_6 q_{yj}^3 \\ + b_7 q_{yj}q_{zj}^2 = pp_y \\ c_1\ddot{q}_{zj} + c_2\dot{q}_{zj} + c_3 q_{zj} + c_4 q_{yj}q_{zj} + c_5 q_{yj}^2 q_{zj} \\ + c_6 q_{zj}^3 = pp_z \\ d_1\ddot{q}_{\theta j} + d_2\dot{q}_{\theta j} + d_3 q_{\theta j} = pp_\theta \end{cases}$$

$$(7)$$

See the appendix for the expressions of coefficients in Equation (7).

III. THEORETICAL FORMULAE FOR MODES AND FREQUENCIES OF MULTISPAN CONDUCTORS

In this paper, the Galerkin method is adopted to transform the partial differential Equation (5) of the galloping transmission line into the ordinary differential Equation (7). However, the specific expression of the mode is not yet known, so Equation(7) cannot be solved. At present, the method to solve the conductor mode is divided into the finite element method and the theoretical method, but the finite element method using discrete elements to solve the conductor mode is not very accurate. In reference [18], in-plane and out-of-plane modes and frequencies of arbitrary multispan conductors were obtained based on the dynamic stiffness theory, and it was pointed out that the calculation method of anti-symmetric modes of multispan conductors was consistent with the calculation method of anti-symmetric modes of Irvine single span conductors. For symmetric modes, the multispan conductors are decomposed into several substructures, and the shape function of each substructure corresponds to the modal function of a single span conductor. This paper uses the mode superposition method to study the galloping characteristics of multispan conductors on the basis of reference [18].

A. IN-PLANE MODES AND FREQUENCIES IN MULTISPAN CONDUCTORS

Equation (7) is also suitable for solving single span conductors. According to reference [11], the symmetrical mode and frequency formula of single-span conductors can be obtained:

$$\psi_y = 1 - \tan(\frac{\bar{\omega}}{2})\sin\frac{\bar{\omega}}{l}x - \cos\frac{\bar{\omega}}{l}x \qquad (8.a)$$

$$1 - (\frac{\lambda}{\omega})^2(1 - \tan(\frac{\bar{\omega}}{2})\frac{2}{\omega}) = 0 \qquad (8.b)$$

In Equation (8.a), ψ_y is the symmetric mode of the single span conductors, $\bar{\omega} = \sqrt{m/H}\omega l$, and $\bar{\omega}$ is the dimensionless frequency, which can be obtained by solving Equation (8.b). In Equation (8.b), $\lambda = (ql/H)\sqrt{EA/H}$.

In reference [18], the in-plane modes and frequencies of multispan conductors are derived based on Irvine's single span suspension cable vibration theory. The in-plane mode expression in any N-span conductor plane is as follows:

$$\psi_{yij} = \begin{cases} \alpha_{1j}^i \sin(\frac{\bar{\omega}_{1j}^i x_1}{2l_1}) \sin(\frac{\bar{\omega}_{1j}^i}{2} - \frac{\bar{\omega}_{1j}^i x_1}{2l_1})/\sin^2(\frac{\bar{\omega}_{kj}^i}{4}) \\ (0 < x_1 < l_1) \\ \alpha_{2j}^i \sin(\frac{\bar{\omega}_{2j}^i x_2}{2l_2}) \sin(\frac{\bar{\omega}_{2j}^i}{2} - \frac{\bar{\omega}_{2j}^i x_2}{2l_2})/\sin^2(\frac{\bar{\omega}_{kj}^i}{4}) \\ (0 < x_2 < l_2) \\ \cdots \\ \alpha_{Nj}^i \sin(\frac{\bar{\omega}_{Nj}^i x_N}{2l_N}) \sin(\frac{\bar{\omega}_{Nj}^i}{2} - \frac{\bar{\omega}_{Nj}^i x_N}{2l_N})/\sin^2(\frac{\bar{\omega}_{kj}^i}{4}) \\ (0 < x_N < l_N) \end{cases}$$

$$(9)$$

The corresponding frequency is obtained by:

$$\sum_{i=1}^{N} \tan(\frac{\bar{\omega}_{kj}^i}{2}) = \frac{1}{2}(1 - (\frac{\bar{\omega}_{1j}^i}{\lambda_1^2})^2)\sum_{i=1}^{N} \bar{\omega}_{kj}^i \qquad (10)$$

In Equation (9), the subscript i of ψ_{yij} indicates that the mode is dominated by the i-th span, and the subscript j represents the number of mode half waves of a single span conductor. $\bar{\omega}_{kj}^i$ is the dimensionless frequency obtained by the parameter of the i-th span conductor. The coefficient $\alpha_{Nj}^i = \cos(\bar{\omega}_{kj}^i/2)/\cos(\bar{\omega}_{Nj}^i/2)$ is used to form the mode vectors into a normalized set of mode shapes.

B. OUT-OF-PLANE MODES AND FREQUENCIES OF MULTISPAN CONDUCTORS

The formulas for solving the out-of-plane mode and frequency of the multispan conductors are related to the span number. Since this paper mainly studies the galloping of multispan conductors with two or three spans, only the formulas of these two cases are listed. The mechanical model of the two-span conductors is proposed (see Fig. 2).

According to substructure theory, reference [18] proposed the out-of-plane mode expression and frequency calculation formula of two-span conductors:

$$\begin{cases} \psi_{z1} = \Delta z \sin(\frac{\bar{\omega}_1 x}{l_1})/\sin(\bar{\omega}_1)(0 < x < l_1) \\ \psi_{z2} = \Delta z \cos(\frac{\bar{\omega}_2 x}{l_2}) - \Delta \bar{z} \cot(\bar{\omega}_2)\sin(\frac{\bar{\omega}_2 x}{l_2})(0 < x < l_2) \end{cases}$$
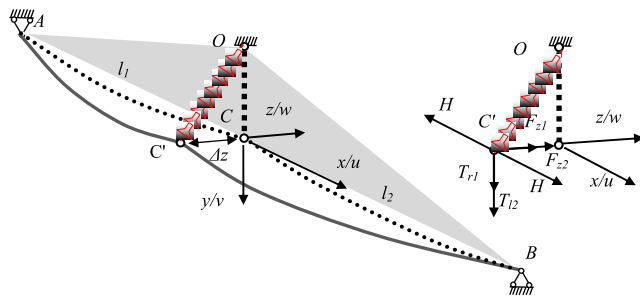
$$(11)$$

FIGURE 2. Mechanical model of two-span conductors.

$$Ha\frac{\bar{\omega}_1}{l_1}[\cot(\bar{\omega}_1) + \cot(\bar{\omega}_2)] + \frac{l_1 + l_2}{2}q - \frac{J\omega^2}{a} = 0 \qquad (12)$$

In Equation (11), Δz is an arbitrary value. As the rotational inertia J of the insulator in Equation (12) is small, $J\omega^2/a$ can be ignored for simplified calculation and solution. The mechanical model of the three-span conductors is shown in Fig. 3.

IV. AERODYNAMIC LOAD OF ICED COVERED CONDUCTORS

A. ESTABLISH AERODYNAMIC LOAD MODEL

Different shapes of iced covered conductors have different aerodynamic characteristics in the air flow. According to actual observations, in an external environment with low temperature and little rain, crescent-shaped ice is easily formed on the surface of the conductors, which is a common ice type in the galloping of iced covered conductors [19].

Based on the galloping mechanism of Nigol, this paper establishes a galloping model of crescent-shaped iced covered conductors, studies the effect of lift, resistance and torque on the conductors under wind load, and makes the following assumptions.

(1) The steady wind blows from left to right along the z-axis horizontally.

(2) The thickness and shape remain constant along the conductors.

(3) Based on quasi-steady theory, the influence of conductor motion on aerodynamic coefficients is not considered [20].

In Fig. 4, P_d and P_l are the drag force and lift force for the iced covered conductor in stable wind. The P_d direction is consistent with the relative wind direction, and the P_l direction is orthogonal to the P_d direction. U is the average wind speed, U_r is the relative wind speed, α is the wind attack angle, and α_0 is the initial wind attack angle.

Obtaining the aerodynamic load of the iced covered conductors is important for studying galloping and its prevention and control technology. In this paper, the dimensionless aerodynamic coefficients of the iced covered conductors are defined according to aerodynamic theory as follows:

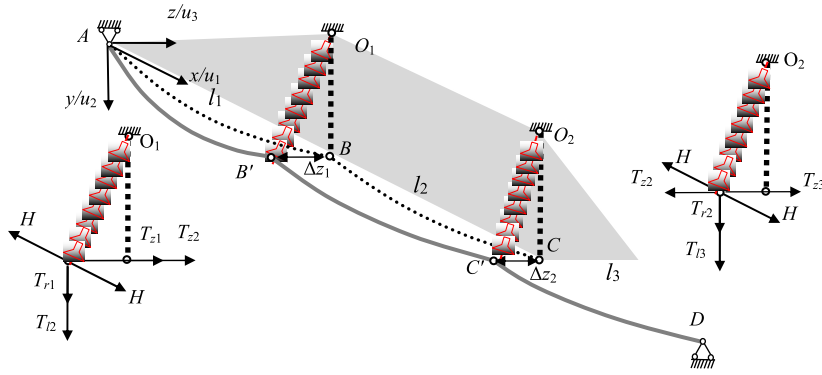$$C_y = \frac{2p_y}{\rho U^2 D}, C_z = \frac{2p_z}{\rho U^2 D}, C_\theta = \frac{2M}{\rho U^2 D^2} \qquad (13)$$

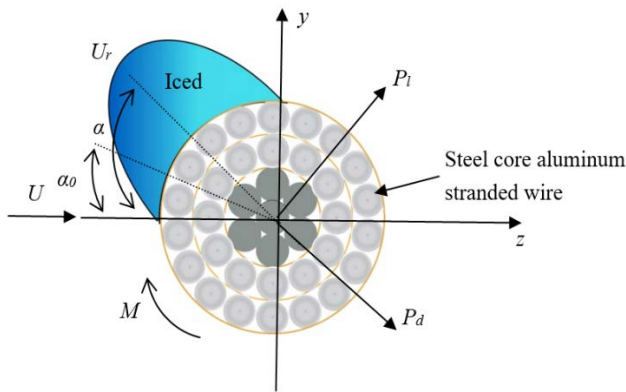**FIGURE 3.** Mechanical model of three-span conductors.

FIGURE 4. Cross section of iced covered conductors.

In Equation (13), C_y, C_z and C_θ are load coefficients, p_y, p_z and M are the lift force, resistance and torque, respectively, ρ is the density of air, and D is the diameter of the bare conductors.

When the average wind blows horizontally toward the iced covered conductors, an initial velocity will be generated due to an initial disturbance on the y-axis of the iced covered conductors, and then there is an angle between the relative wind speed and the real wind speed. The change in the angle of attack during the galloping of crescent-shaped iced covered conductors can be expressed as:

$$\alpha = \alpha_0 + \theta - \frac{\dot{u}_2 + \frac{1}{2}\dot{\theta}D}{U} \approx \theta - \frac{\dot{u}_2}{U} \quad (14)$$

In Equation (14), θ is the dynamic angle.

B. AERODYNAMIC COEFFICIENT
The third-order Taylor expansion of C_y, C_z, and C_θ can be obtained:

$$\begin{cases} C_y = \lambda_1\alpha + \lambda_2\alpha^2 + \lambda_3\alpha^3 \\ C_z = \lambda_4\alpha + \lambda_5\alpha^2 + \lambda_6\alpha^3 \\ C_\theta = \lambda_7\alpha + \lambda_8\alpha^2 + \lambda_9\alpha^3 \end{cases} \quad (15)$$

See the appendix for the expressions of coefficients in Equation (15).

According to reference [14], the aerodynamic coefficient can be obtained at wind speed $U = 8.5$ m/s and wind attack angle $\alpha = 180°$ as follows:

$$\begin{cases} C_y = -2.0821\alpha - 0.0288\alpha^2 + 5.0779\alpha^3 \\ C_z = -0.6644\alpha - 0.2196\alpha^2 + 0.3095\alpha^3 \\ C_\theta = 0.1874\alpha + 0.6924\alpha^2 + 0.0323\alpha^3 \end{cases} \quad (16)$$

Substitute Equation (14) into Equation (15) to obtain the lift and drag in the y and z directions:

$$\begin{cases} p_y = \frac{1}{2}\rho U^2 D[\lambda_1(-\frac{\dot{u}_2}{U}) + \lambda_2(-\frac{\dot{u}_2}{U})^2 + \lambda_3(-\frac{\dot{u}_2}{U})^3] \\ p_z = \frac{1}{2}\rho U^2 D[\lambda_4(-\frac{\dot{u}_2}{U}) + \lambda_5(-\frac{\dot{u}_2}{U})^2 + \lambda_6(-\frac{\dot{u}_2}{U})^3] \\ M = \frac{1}{2}\rho U^2 D^2[\lambda_7(-\frac{\dot{u}_2}{U}) + \lambda_8(-\frac{\dot{u}_2}{U})^2 + \lambda_9(-\frac{\dot{u}_2}{U})^3] \end{cases} \quad (17)$$

Substitute Equation (17) into Equation (7) to obtain the ordinary differential equations of the coupled vibration of three degrees of freedom:

$$\begin{cases} b_1\ddot{q}_2 + \bar{b}_2\dot{q}_2 + b_3q_2 + b_4q_2^2 + b_5q_3^2 + b_6q_2^3 \\ + b_7q_2q_3^2 + b_9\dot{q}_2^2 + b_{10}\dot{q}_2^3 = 0 \\ c_1\ddot{q}_3 + c_2\dot{q}_3 + c_3q_3 + c_4q_2q_3 + c_5q_2^2q_3 \\ + c_6q_3^3 + c_8\dot{q}_2 + c_9\dot{q}_2^2 + c_{10}\dot{q}_2^3 = 0 \\ d_1\ddot{q}_\theta + d_2\dot{q}_\theta + d_3q_\theta + d_4\dot{q}_2 + d_5\dot{q}_2^2 + d_6\dot{q}_2^3 = 0 \end{cases} \quad (18)$$

The expressions of coefficients in Equation (18) are given in the Appendix.

V. MULTIPLE SCALE METHOD FOR SOLVING NONLINEAR EQUATIONS
The multiple scale method is one of the most important methods to study nonlinear problems [21]. It is widely used not only for strict periodic motion but also for attenuated vibration of dissipative systems and many other occasions. The galloping problem of iced covered conductors belongs

to a weak nonlinear vibration problem. For the analysis of weak nonlinear problems, the steady-state response and transient response can be calculated by the multiple scale method.

Before solving nonlinear differential equations with the multiple scale method, this paper simply changes the form of the two-degree-of-freedom nonlinear coupled vibration Equation (18) as follows:

$$
\begin{cases}
\ddot{q}_y + b'_1\dot{q}_y + \omega_y^2 q_y + b'_2 q_y^2 + b'_3 q_z^2 + b'_4 q_y^3 + \\
b'_5 q_y q_z^2 + b'_7 \dot{q}_y^2 + b'_8 \dot{q}_y^3 = 0 \\
\ddot{q}_z + c'_1\dot{q}_z + \omega_z^2 q_z + c'_2 q_y q_z + c'_3 q_y^2 q_z + \\
c'_4 q_z^3 + c'_6 \dot{q}_y + c'_7 \dot{q}_y^2 + c'_8 \dot{q}_y^3 = 0
\end{cases}
\tag{19}
$$

See the appendix for the expressions of coefficients in Equation (19).

The nonlinear term in the finishing Equation (20) can be obtained as follows:

$$
\begin{cases}
\ddot{q}_y + \omega_y^2 q_y + \varepsilon(b'_1\dot{q}_y + b'_2 q_y^2 + b'_3 q_z^2 + b'_4 q_y^3 \\
+ b'_5 q_y q_z^2 + b'_7 \dot{q}_y^2 + b'_8 \dot{q}_y^3) = 0 \\
\ddot{q}_z + \omega_z^2 q_z + \varepsilon(c'_1\dot{q}_z + c'_2 q_y q_z + c'_3 q_y^2 q_z \\
+ c'_4 q_z^3 + c'_6 \dot{q}_y + c'_7 \dot{q}_y^2 + c'_8 \dot{q}_y^3) = 0
\end{cases}
\tag{20}
$$

In Equation (20), q_y and q_z represent the displacement in the y-direction and z-direction, respectively. ω_y and ω_z are the circular frequencies in the y-direction and z-direction, respectively. ε is a small dimensionless parameter.

The displacement can be expressed as the following function:

$$
\begin{cases}
q_y(t) = q_{y0}(T_0, T_1) + \varepsilon q_{y1}(T_0, T_1) + \varepsilon^2 \cdots \\
q_z(t) = q_{z0}(T_0, T_1) + \varepsilon q_{z1}(T_0, T_1) + \varepsilon^2 \cdots
\end{cases}
\tag{21}
$$

The variables $T_0 = t$ and $T_1 = \varepsilon t$ of the time scale are introduced into Equation (21).

The velocity and acceleration of iced covered conductors can be obtained by taking the first-order and second-order derivatives of Equation (21):

$$
\begin{cases}
\dot{q}_y = D_0 q_{y0} + \varepsilon(D_1 q_{y0} + D_0 q_{y1}), \\
\dot{q}_z = D_0 q_{z0} + \varepsilon(D_1 q_{z0} + D_0 q_{z1}) \\
\ddot{q}_y = D_0 q_{y0} + \varepsilon(2D_0 D_1 q_{y0} + D_0^2 q_{y1}) \\
\ddot{q}_z = D_0 q_{z0} + \varepsilon(2D_0 D_1 q_{z0} + D_0^2 q_{z1})
\end{cases}
\tag{22}
$$

Substituting Equation (22) into Equation (19) and equating the coefficients of the similar terms of ε, we can obtain the following set of linear differential equations:

$$
\varepsilon^0 : \begin{cases}
D_0^2 q_{y0} + \omega_y^2 q_{y0} = 0 \\
D_0^2 q_{z0} + \omega_z^2 q_{z0} = 0
\end{cases}
\tag{23}
$$

$$
\varepsilon^1 : \begin{cases}
D_0^2 q_{y1} + \omega_y^2 q_{y1} = -2D_0 D_1 q_{y0} + b'_1 D_0 q_{y0} \\
+ b'_2 q_{y0}^2 + b'_3 q_{z0}^2 + b'_4 q_{y0}^3 + b'_5 q_{y0} q_{z0}^2 \\
+ b'_7 (D_0 q_{y0})^2 + b'_8 (D_0 q_{y0})^3 \\
D_0^2 q_{z1} + \omega_z^2 q_{z1} = -2D_0 D_1 q_{z0} + c'_1 D_0 q_{z0} \\
+ c'_2 q_{y0} q_{z0} + c'_3 q_{y0}^2 q_{z0} + c'_4 q_{z0}^3 + \\
c'_6 (D_0 q_{y0}) + c'_7 (D_0 q_{y0})^2 + c'_8 (D_0 q_{y0})^3
\end{cases}
\tag{24}
$$

The periodic solution adopted as the solution to Equation(23) is as follows:

$$
\begin{cases}
q_{y0} = A_y(T_1)e^{i\omega_y T_0} + cc \\
q_{z0} = A_z(T_1)e^{i\omega_z T_0} + cc
\end{cases}
\tag{25}
$$

In Equation (25), i is an imaginary number and cc denotes the complex conjugates of $A_y(T_1)e^{i\omega_y T_0}$, $A_z(T_1)e^{i\omega_z T_0}$. Then, substitute Equation (25) into the system of equations of order ε^1:

$$
\begin{cases}
D_0^2 q_{y1} + \omega_y^2 q_{y1} = -2i\omega_y D_1 A_y e^{i\omega_y T_0} + b'_1 i\omega_y A_y e^{i\omega_y T_0} \\
+ b'_2(A_y^2 e^{2i\omega_y T_0} + 2A_y\bar{A}_y) + b'_3(A_z^2 e^{2i\omega_z T_0} + A_z\bar{A}_z) \\
+ b'_4(A_y^3 e^{3i\omega_y T_0} + 3A_y^2\bar{A}_y e^{i\omega_y T_0}) + b'_5(A_y A_z^2 e^{i(2\omega_z+\omega_y)T_0} \\
+ 2A_y A_z\bar{A}_z e^{i\omega_y T_0} + A_y\bar{A}_z^2 e^{i(-2\omega_z+\omega_y)T_0}) + b'_7(-\omega_y^2 \\
A_y^2 e^{2i\omega_y T_0} + 2\omega_y^2 A_y\bar{A}_y) + b'_8(-i\omega_y^3 A_y^3 e^{3i\omega_y T_0} \\
+ 3i\omega_y^3 A_y^2\bar{A}_y e^{i\omega_y T_0}) + cc \\
D_0^2 q_{z1} + \omega_z^2 q_{z1} = -2i\omega_y D_1 A_z e^{i\omega_z T_0} + c'_1 i\omega_z A_z e^{i\omega_z T_0} \\
+ c'_2(A_y A_z e^{i(\omega_z+\omega_y)T_0} + A_y\bar{A}_z e^{i(\omega_y-\omega_z)T_0}) + c'_3(A_z \\
A_y^2 e^{i(2\omega_y+\omega_z)T_0} + 2A_z A_y\bar{A}_y e^{i\omega_z T_0} + A_z\bar{A}_y^2 e^{i(-2\omega_y+\omega_z)T_0}) \\
+ c'_4(A_z^3 e^{3i\omega_z T_0} + 3A_z^2\bar{A}_z e^{i\omega_z T_0}) + c'_6 i\omega_y A_y e^{i\omega_y T_0} + \\
c'_7(-\omega_y^2 A_y^2 e^{2i\omega_y T_0} + 2\omega_y^2 A_y\bar{A}_y) + c'_8(-i\omega_y^3 \\
A_y^3 e^{3i\omega_y T_0} + 3i\omega_y^3 A_y^2\bar{A}_y e^{i\omega_y T_0}) + cc
\end{cases}
\tag{26}
$$

Eliminating the secular terms in q_{y1} and q_{z1} gives:

$$
\begin{cases}
(-2i\omega_y D_1 A_y + b'_1 i\omega_y A_y + b'_4 3A_y^2\bar{A}_y + \\
b'_5 2A_y A_z\bar{A}_z + b'_8 3i\omega_y^3 A_y^2\bar{A}_y)e^{i\omega_y T_0} = 0 \\
(-2i\omega_y D_1 A_z + c'_1 i\omega_z A_z + c'_3 2A_z A_y\bar{A}_y + \\
c'_4 3A_z^2\bar{A}_z)e^{i\omega_z T_0} = 0
\end{cases}
\tag{27}
$$

Assume that $A_y(T_1)$ and $A_z(T_1)$ are expressed as follows:

$$
\begin{cases}
A_y(T_1) = \frac{1}{2}a_y(t)e^{i\theta_y(t)} \\
A_z(T_1) = \frac{1}{2}a_z(t)e^{i\theta_z(t)}
\end{cases}
\tag{28}
$$

In Equation (28), a_y and a_z are the amplitudes of galloping, and θ_y and θ_z are the phases.

We substitute Equation (28) into Equation (27) and separate the real and imaginary parts to obtain:

$$
\begin{cases}
\dot{a}_y = \frac{1}{2}a_y b'_1 + \frac{3}{8}a_y^3\omega_y^2 b'_8 \\
\dot{\theta}_y = -(\frac{3}{8\omega_y}b'_4 a_y^2 + \frac{1}{4\omega_y}b'_5 a_z^2) \\
\dot{a}_z = \frac{1}{2}a_z c'_1 \\
\dot{\theta}_z = -(\frac{1}{4\omega_z}c'_3 a_y^2 + \frac{3}{8\omega_z}c'_4 a_z^2)
\end{cases}
\tag{29}
$$

If the right side of each Equation (29) is zero, the steady-state amplitude of the iced covered conductors can be obtained.

Integrating Equation (29) with time yields:

$$
\begin{cases}
a = \dfrac{1}{\sqrt{\left(\frac{1}{a_0^2} + \frac{n}{p}\right)e^{-2pt} - \frac{n}{p}}} \\[2ex]
\theta = \{-\dfrac{1}{8\omega_y}(\bar{b}_2 - b_2)^2 - \dfrac{\bar{b}_2 - b_2}{4\omega_y}\mu_y + \\[1ex]
\quad [(-\dfrac{5}{12\omega_y^3}b_2'^2 + \dfrac{3}{8\omega_y}b_4') - \dfrac{1}{2\omega_y^2}b_2'b_8']\dfrac{p}{pe^{-2pt} - n}\}t
\end{cases}
$$

$$(30)$$

In Equation (30), $p = -\frac{\bar{b}_2 - b_2}{2} - \frac{\mu_y}{2}$; $n = -\frac{3b_8'}{8}\omega_y^2$, a_0 is the initial value.

The approximate solutions of the multiple scales method of the solution form of the first-order small parameter (T_0 and T_1) are [22]:

$$
q_y = a\cos(\psi) + a^2\left[\frac{b_2'}{6\omega_y^2}\cos(2\psi) - \frac{b_2'}{2\omega_y^2}\right]
$$

$$
+ \left[\left(\frac{b_2'^2}{48\omega_y^4} + \frac{b_4'}{32\omega_y^2}\right)a^3\cos(3\psi) \right.
$$

$$
\left. + \frac{1}{9\omega_y^3}b_2'(\bar{b}_2 - b_2)a^2\sin(3\psi) \right]
$$

$$(31)$$

In Equation (31), $\psi = \omega_y t + \theta$.

Equation (31) is the analytical solution of the conductors. It is faster to use the analytical solution to obtain the displacement time-history curve of the conductors than the numerical solution.

VI. NUMERICAL EXAMPLES AND RESULT ANALYSIS

The galloping characteristics of multispan ice-covered conductors are mainly related to the length of span, the initial tension and the number of spans. When the number of spans is second or third, the multispan conductor model can accurately reflect the influence of adjacent spans on the overall galloping of the conductors in a tension section. This paper studies the galloping characteristics of ice-covered conductors under changes in these structural parameters. Since it is very difficult to solve the analytical solution of dynamic Equation (21) according to the theory of current nonlinear dynamics, in this paper, the fourth-order Runge–Kutta method is used to solve Equation (21). To verify the accuracy of the model in this paper, the same structural parameters as those in reference [14] were selected. The specific physical parameters of the conductors are shown in Table 1, with a length of 125 m, an initial tension of 15 kN for single conductors, and a length of 2.1 m and a weight of 490 N for each insulator string connected to the conductors.

A. VERIFY THE PROPOSED GALLOPING MODEL

According to actual field observations of galloping, there is torsional motion in conductor galloping [23], so some studies add the influence of torsional freedom on conductor galloping [24], [25], but some studies only establish a two-degree-of-freedom model [26], [27]. These two studies based on the Niol galloping mechanism and Den Hartog galloping mechanism have been accepted, but increasing the degree of freedom will increase the amount of calculation. Therefore, this paper first carries out numerical simulation of ice-covered single span conductors (initial tension 15 kN) with 3-DOF and 2-DOF lower span spacing of 125 m and compares the influence of different degrees of freedom on the galloping characteristics of single span conductors.

Equation (8) is used to obtain the modal and frequency of the single span conductors. The parameters and modal in Table 1 are put into Equation (19), and the time-history curves of the displacement of the single span conductors with 3-DOF and 2-DOF can be obtained by using the fourth order Runge–Kutta method, as shown in Fig. 5.

Fig. 5 shows that the in-plane amplitude of the 3-DOF singlespan conductors is 0.294 m and that of the 2-DOF single-span conductors is 0.301 m by the fourth order Runge–Kutta method. The out-of-plane amplitude was 0.009 m for 3-DOF and 0.009 m for 2-DOF. Therefore, joint torsional degrees of freedom can reduce the conductor wave amplitude, but with three degrees of freedom, calculating conductors galloping for a long time, and the two-degree-offreedom model can also be a very good reaction adjacent to spans, leading to multiple lead wave characteristics. The influence of torsion energy does not occur through the insulator to the adjacent spans, so this is does not consider the effect of torsion.

The time-history curves of in-plane displacement within 10 s after the single span conductors tend to be stable in the literature [14]. Fig. 6 shows the calculation results of the finite element method, the multiscale method and the 2 degrees of freedom of this paper.

As shown in Fig. 6, the conductor frequency in reference [13] is 0.70 Hz, and the conductor frequency in this study is 0.68 Hz. The frequencies obtained by these two calculation methods are very close. However, Desai used finite element software to establish a single-file model and found that the in-plane amplitude was approximately 0.2 m [14]. There may be several reasons for this difference. First, Desai adopted a modal decomposition method based on linear assumptions to solve the dynamic equation, ignoring the geometric nonlinearity caused by the large galloping of the conductors, while the Runge–Kutta method was used to calculate nonlinear problems with higher accuracy. Second, the finite element method used the damping ratio as a whole mode, but multiple modes would be excited, and the change in damping ratio had a great influence on the amplitude. Finally, some errors may also occur when reading the data of the time-history curves of single conductor displacements in the literature [14].

In this study, the in-plane amplitude of the 2-DOF single span conductors is 0.288 m by using the multiple scale method. The results obtained by the multiple scale method are very close to those obtained by the fourth order Runge–Kutta

TABLE 1. Physical parameters of transmission lines.

Parameters	Notation	Units	For line in example1
Axial rigidity	AE	10^6N	25.53
Diameter of bare cable	d	10^{-3}m	23.5
Damping ratio in the y direction	ζ_y	10^{-2}	1.6
Damping ratio in the z direction	ζ_z	10^{-2}	1.6
Damping ratio in the θ direction	ζ_θ	10^{-2}	5.7
Mass per unit length	m	kg $\cdot$ m^{-1}	1.66
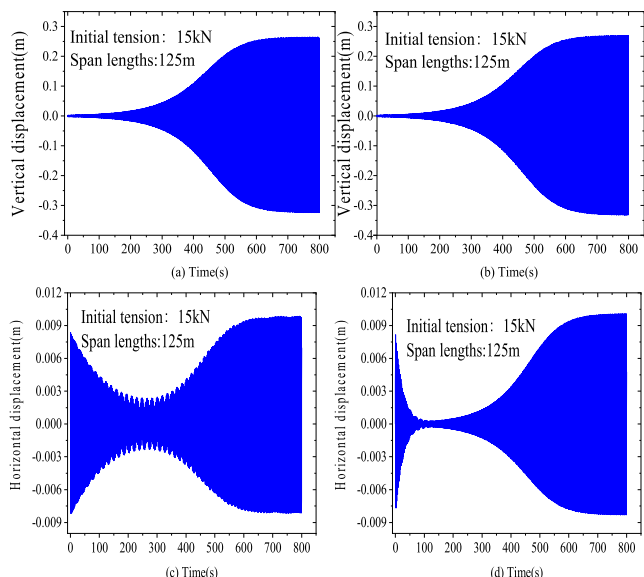
FIGURE 5. Displacement time-history curves of single-span conductors with different degrees of freedom: (a), (c) three degrees of freedom; (b), (d) two degrees of freedom.

method, which also shows that the results obtained by the model in this paper are accurate.

B. ANALYSIS OF GALLOPING CHARACTERISTICS OF SINGLE CONDUCTORS

In this paper, single-span conductors with 100 m span length and 15 kN initial tension are first selected to study the difference between single-span conductors and multispan conductors and the influence of the span number on the galloping characteristics of the conductors. Other parameters are shown in Table 1. To verify the accuracy of the theoretical formula calculated in this paper, Abaqus finite element software was used to establish the corresponding model to calculate the frequency and mode. A cable element was used to simulate the cable, and a rod element was used to simulate the insulator string. The number of grids was 100. The first three order symmetric modes and frequencies of the single span conductors plane calculated by theoretical Equation (8) and finite element software are shown in Table 2.

Table 2 shows that the results obtained by the two calculation methods are very close, so the conductor model established by Abaqus in this paper is also accurate. The

results of the first-order in-plane symmetric modal frequency calculated by the theoretical formula in Table 2 are substituted into Equation (19), and the displacement time-history curves of a single-span conductor with a length of 100 m (initial tension 15 kN) are obtained, as shown in Fig. 7.

Fig. 7 shows that the in-plane amplitude of the single-span conductors is 0.154 m and the out-of-plane amplitude is 0. 006 m. According to the frequency analysis of the characteristics of in-plane galloping of the single-span conductors, the frequency is 0.762 Hz before the single-span conductors tends to be stable and 0.755 Hz after it tends to be stable. The frequency calculated by the fourth-order Runge–Kutta method is very close to the first-order frequency of 0.764 Hz calculated by the finite element method. Therefore, the frequency of the single-span conductors does not change greatly from the beginning of galloping to stabilizing.

To compare the difference between the galloping characteristics of multispan conductors and single-span conductors after the initial tension increases, the displacement time-history curves of single-span conductors after the initial tension gradually increases are given in Fig. 8.

Fig. 8 shows that the amplitude of the single-span conductors increases first and then decreases with increasing initial tension.

C. ANALYSIS OF GALLOPING CHARACTERISTICS OF TWO-SPAN CONDUCTORS

1) EFFECT OF SPAN LENGTH ON THE GALLOPING OF TWO-SPAN CONDUCTORS WITH UNEQUAL SPAN LENGTH

In this study, the length of the first-span conductors is kept constant, and the length of the second-span conductors is gradually increased to analyze the influence of the length between adjacent spans on the galloping characteristics of the two spans. The length of the two conductors is set to 100 m-50 m, 100 m-80 m, 100 m-150 m, and 100 m-200 m, and the initial tension is 15 kN; see Table 1 for other parameters. The frequency and mode of the two-span conductors obtained by theoretical Equations (10) and (12) and the Abaqus solution are shown in Table 3.

Table 3 shows that the results of the theoretical solution and finite element solution are basically the same, and the existing errors are within a reasonable range, thus proving the accuracy and precision of the calculation results by using the theoretical formula. The in-plane and out-of-plane
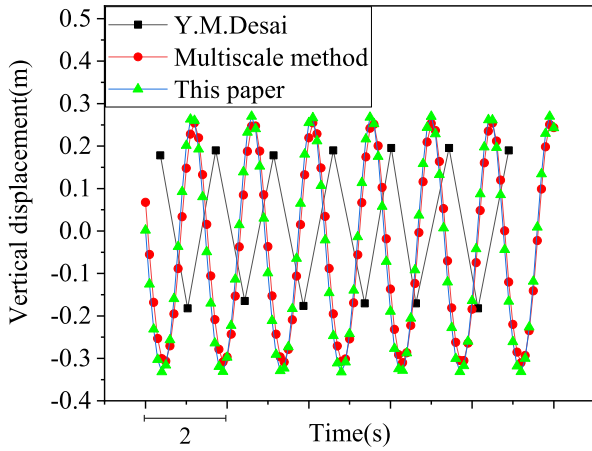
FIGURE 6. Displacement time-history curves of single span transmission lines in the two studies (initial tension is 15 kN, single span length of 125 m).

TABLE 2. Frequency and mode of 100 m length single span conductors (initial tension 15 kN).

The mode shape obtained by the theoretical formula	Calculation method	Frequency（Hz）
First order in-plane symmetric modal frequency	Theoretical formula	0.765
	Abaqus	0.764
Third order in-plane symmetric modal frequency	Theoretical formula	1.443
	Abaqus	1.442
Fifth order in-plane symmetric modal frequency	Theoretical formula	2.379
	Abaqus	2.376

frequencies of the two-span conductors decrease gradually when the length between adjacent spans increases gradually, and the frequency of the two-span conductors is obviously lower than that of the single-span conductors. The modes drawn using theoretical Equation (9) are shown in Fig. 9.

Fig. 9 shows that the modal shapes of the first span conductors are basically the same. With the increase in the length of the second-span conductors, the amplitude of the mode of the second-span conductors gradually increases. Limited by space, this paper only gives the conductor modal diagram calculated by the finite element method when the length of the two-span conductors is 100 m-200 m, as shown in Fig. 10.

Fig. 10 shows that the modal shapes obtained by Abaqus are basically consistent with Fig. 9, so the modes in Fig. 9 are also accurate.

Substituting the first-order normalized symmetric modal frequency in Table 3 into Equation (19), the fourth-order
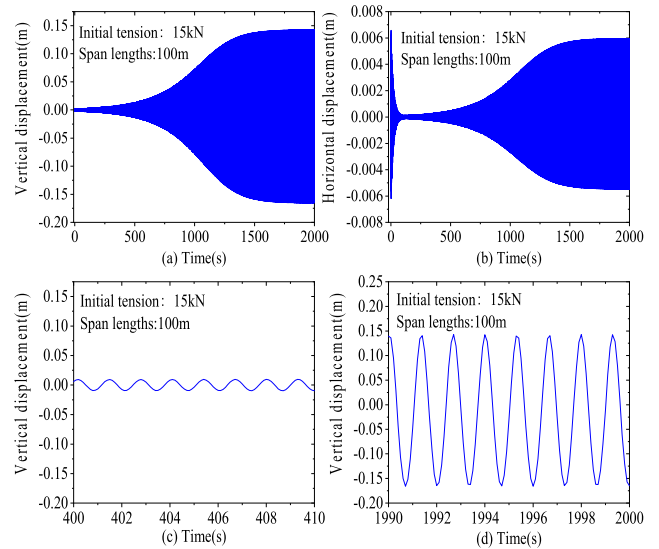
FIGURE 7. Displacement time-history curves of single span transmission lines.
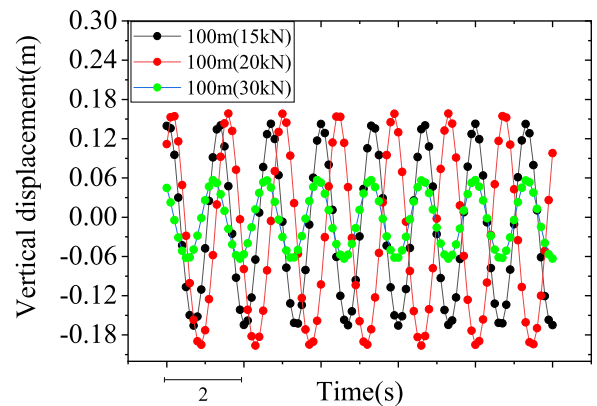

FIGURE 8. Displacement time-history curves of single-span conductors (different initial tensions).

TABLE 3. Frequency of two unequal-pitch conductors with an initial tension of 15 kN.

Span(m)		100-50	100-80	100-150	100-200
Mode type	Method		Frequency(Hz)		
first-order in-plane symmetric modes	theoretical solution	0.647	0.534	0.405	0.385
	Abaqus	0.647	0.534	0.406	0.385
first order out-of-plane symmetric modes	theoretical solution	0.396	0.380	0.285	0.223
	Abaqus	0.392	0.377	0.286	0.224

Runge–Kutta method was used to solve, and the displacement time-history curves of unequal length two-span conductor galloping were obtained, as shown in Fig. 11.

Fig. 11 shows that the galloping time of the two-span conductors tends to stabilize and gradually decrease
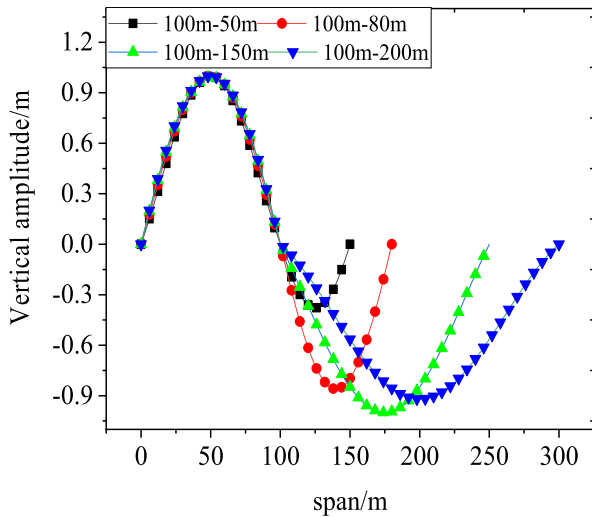
FIGURE 9. Mode diagram of two-span transmission lines with unequal span lengths.

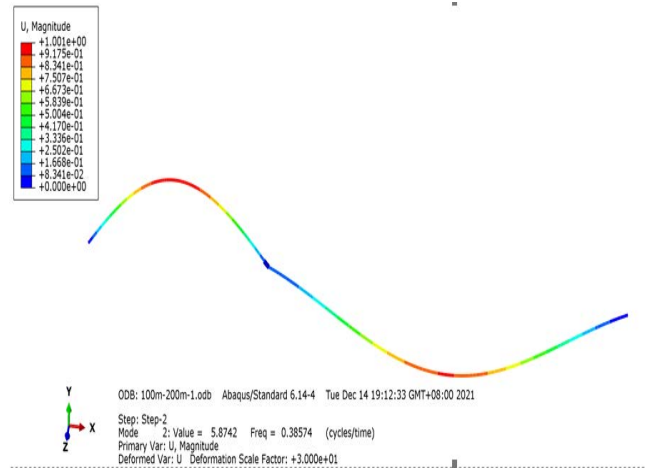FIGURE 10. Two-span conductor modes obtained by the finite element method.

with increasing length of the second-span conductors. The in-plane amplitude is 0.841 m in 100 m-50 m, 1.174 m in 100 m-80 m, 1.736 m in 100 m-150 m, and 1.876 m in 100 m-200 m. The amplitude in the plane between 100 m-200 m is 2.084 m by using the multiscale method. The amplitudes of the multispan conductors obtained by the two methods are relatively close, so the model for calculating the two-span conductors in this paper is also accurate.

The amplitude of the two-span conductors with lengths of 100 m-50 m is significantly greater than that of the single-span conductors with lengths of 100 m. This is because the energy of the two-span conductors will be transmitted to the adjacent conductors through the insulator string, resulting in a greater amplitude. Therefore, it is necessary to study the galloping of multispan conductors in practical engineering. In addition, in-plane galloping is mainly the galloping of multispans conductors [2]. To more clearly compare the effect of increasing the length of adjacent spans on amplitude, the time-history curves of displacement within 10 s are selected when the galloping of two-span conductors is stable, as shown in Fig. 12.

Fig. 12 shows that the amplitude of multiple conductors with adjacent spans increases with increasing span. According to the single degree of freedom of the wave amplitude Equation $A = 2\mu/(\sqrt{3}\omega_0)$, the greater the conductor circular frequency is, the smaller the amplitude (where A is the amplitude, μ is related to wind speed and the conductor aerodynamic parameter parameters, and ω_0 is the circular frequency of the conductors). These results are consistent with the conclusion of the formula in this paper.

Studying the galloping trace of ice-covered conductors can provide an important basis for galloping mechanisms and antigalloping measures. The galloping traces of the two-span conductors with unequal span lengths are shown in Fig. 13.

Fig. 13 shows that galloping is mainly in the vertical direction, and the trajectory is approximately oval. This is
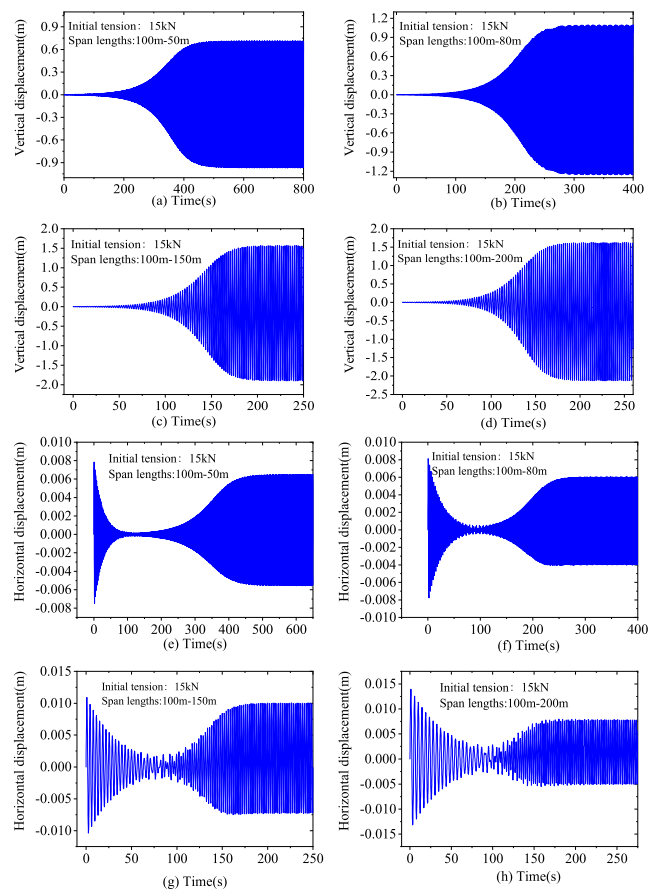
FIGURE 11. Displacement time-history curves of two-span transmission lines with nonequal span length.

consistent with the galloping form described by the galloping mechanism widely recognized in the current galloping research field; that is, galloping is a process of gradual formation. At the initial span, the conductors oscillate with a small amplitude near the equilibrium position. Due to the accumulation of wind energy and the negative damping of
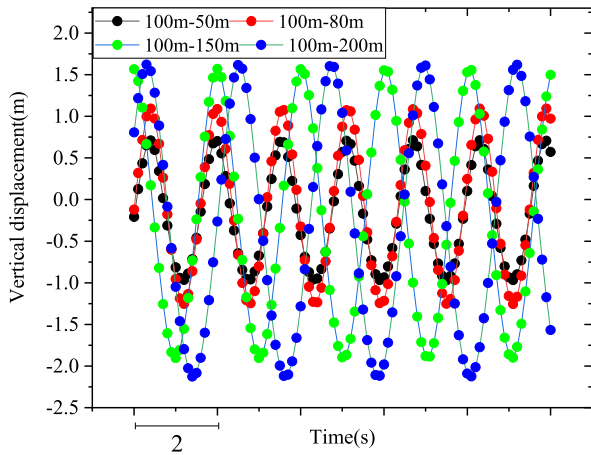
FIGURE 12. Displacement time-history curves of two-span transmission lines with unequal span length (initial tension is 15 kN).

FIGURE 13. Galloping trace of two-span transmission lines with unequal span length under different spans.

air, the horizontal amplitude gradually decreases. At the same time, the vertical amplitude increases, forming an ever-larger elliptic galloping trajectory, which eventually tends to be stable due to the influence of system damping. This also proves the correctness of the numerical simulation.

The circular frequency of the single-span conductors is almost unchanged before and after galloping is stable. Now, the displacement time-history curves of the two-span conductors with lengths of 100 m-200 m are selected for 10 s before and after galloping is stable, as shown in Fig. 14.

Fig. 14 shows that the frequencies of the two-span conductors before and after galloping tend to be stable are 0. 389 Hz and 0.449 Hz, respectively. The frequency obtained by using Abaqus is 0.385 Hz, which is very close to the frequency obtained by the fourth-order Runge-Kuta method before conductor galloping tends to be stable. However, with increasing conductor galloping time, the frequency will increase after conductor galloping tends to be stable. This is because the influence of the nonlinear term causes the in-plane frequency of the two-span conductors to increase when they are galloping.

2) EFFECT OF SPAN LENGTH ON THE GALLOPING OF TWO-SPAN CONDUCTORS WITH EQUAL SPAN LENGTH

It is a special case that the length of each conductor in two spans is the same because the conductor frequency is the same. In this paper, two-span conductors with equal span lengths are selected for study. The frequency after the change in the length of the two-span conductors is shown in Table 4, and the other parameters remain unchanged.

Table 4 shows that the frequencies of the two-span conductors with equal span lengths are also very accurate. As the span length of the two-span conductors with equal span length increases, the frequency gradually decreases. The modes drawn using theoretical Equation (9) are shown in Fig. 15.

Fig. 15 shows that when the conductor spacing is equal, it has the same shape. With the increase in the second
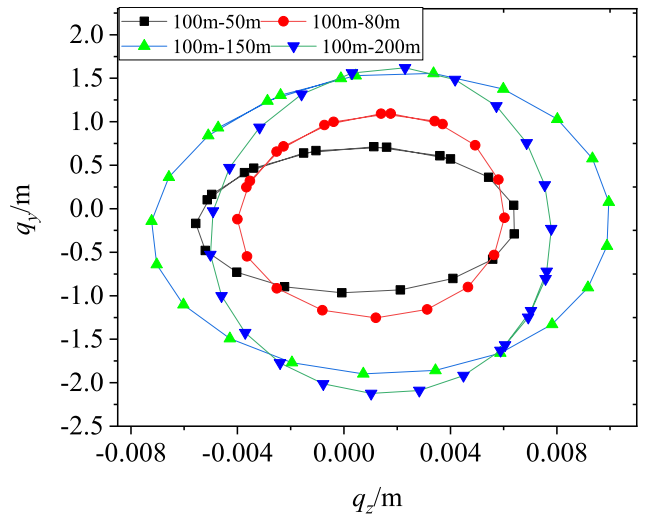
conductor length, there are two downward half waves in the conductor mode because the sag increases with increasing length.

Substitute the first-order in-plane symmetric modal frequency results calculated by the theoretical formula in Table 4 into Equation (19) and obtain the time-history curves of the two-span conductor displacement at different spans (initial tension 15 kN), as shown in Fig. 16.

Fig. 16 shows that the time when the two-span conductors with equal length gallops stabilize gradually decreases with the simultaneous increase in the length between the two conductors. The in-plane amplitude of the two-span conductors with lengths of 80 m-80 m is 0.878 m, and that of the two-span conductors with lengths of 100 m-100 m is 1.378 m. The in-plane amplitude of the two-span conductors with lengths of 150 m-150 m is 2.391 m, and that of the two-span conductors with lengths of 200 m-200 m is 3.466 m.

When the total span of the two-span conductors is 300 m, the in-plane amplitude of the two conductors increases by 27.45% after the nonequal two-span conductors with distances of 100 m-200 m are changed into equal two-step conductors with distances of 150 m-150 m. Although the total span distance does not change, the amplitude will continue to increase when the frequencies of the two conductors are close.

To more clearly compare the effect of increasing the conductor spacing on the vertical amplitude, the displacement time-history curves within 10 s are selected when the two-span conductors with equal span length are galloping steadily, as shown in Fig. 17.

Fig. 17 shows that the amplitude of the two spans with equal span length increases with increasing conductor length. Therefore, regardless of whether the child traverse length is the same, the amplitude of the two spans will increase when the length of one of the two spans increases or the length of the two spans increases simultaneously.

TABLE 4. Frequency of two-span conductors with equal pitch and initial tension of 15 kN.

Span(m)		80-80	100-100	150-150	200-200
Mode type	Method		Frequency(Hz)		
first order in-plane symmetric mode	Theoretical formula	0.597	0.477	0.317	0.238
	Abaqus	0.595	0.476	0.315	0.241
first order out-of-plane symmetric mode	Theoretical formula	0.442	0.363	0.257	0.201
	Abaqus	0.440	0.360	0.274	0.218
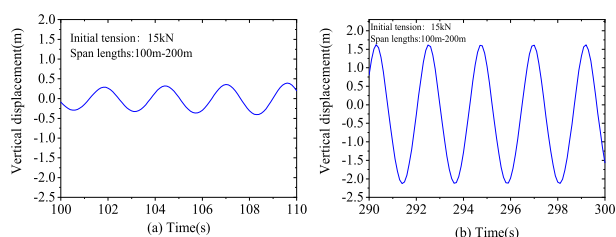
FIGURE 14. Displacement time-history curves before and after galloping stability of two-span transmission lines (two-span length of 100 m -200 m).
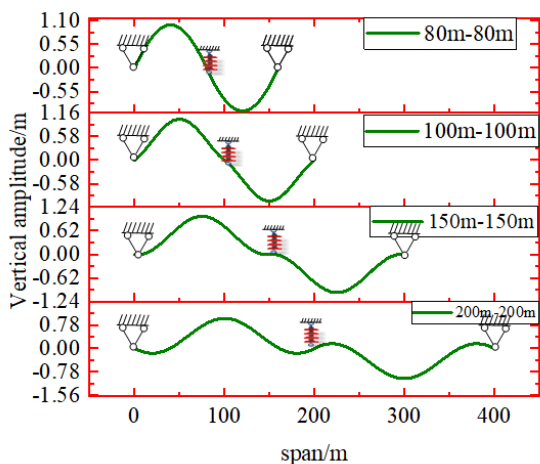
FIGURE 15. Mode diagram of two-span transmission lines with equal span length.

The galloping tracks of the two-span conductors with equal span lengths are shown in Fig. 18.

Fig. 18 shows that when the length between the conductors increases simultaneously, the vertical amplitude of the two-span conductors increases significantly, while the horizontal amplitude does not change significantly.

3) EFFECT OF INITIAL TENSION ON THE GALLOPING OF TWO-SPAN CONDUCTORS WITH EQUAL SPAN LENGTH

The mode and frequency of the conductors will also change after the initial tension of the conductors change. Next, two kinds of common initial tension of the conductors are selected
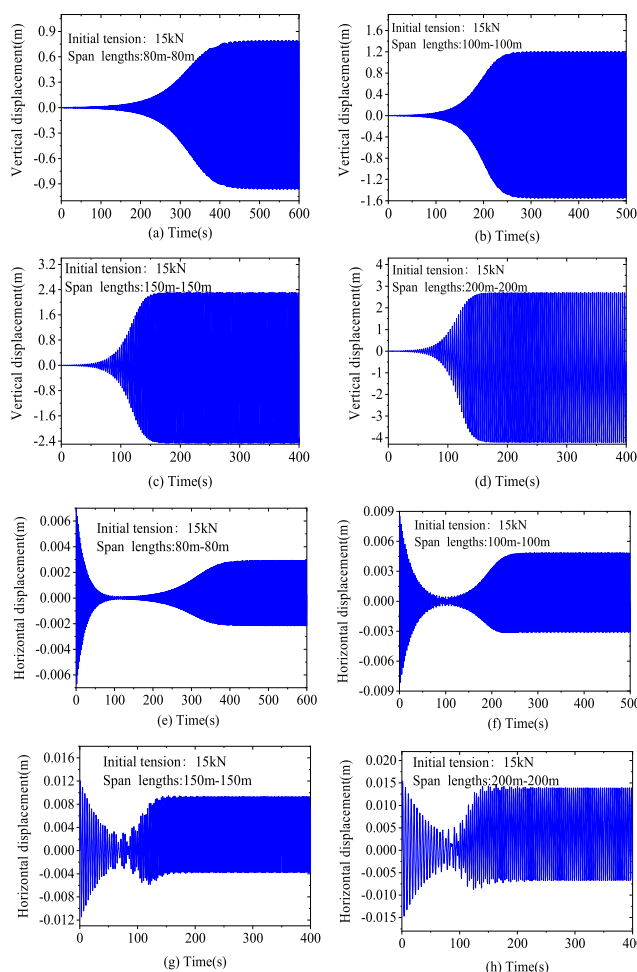

FIGURE 16. Displacement time-history curves of two-span transmission lines with equal span length.

in this paper to study the influence of different initial tensions on the galloping characteristics of the two-span conductors with span lengths of 100 m-100 m. The frequencies of the two-span conductors under the two initial tensions are shown in Table 5.

Table 5 shows that the results calculated using the theoretical formula are accurate. The frequency of the equal-span two-span conductors increases with increasing initial tension.
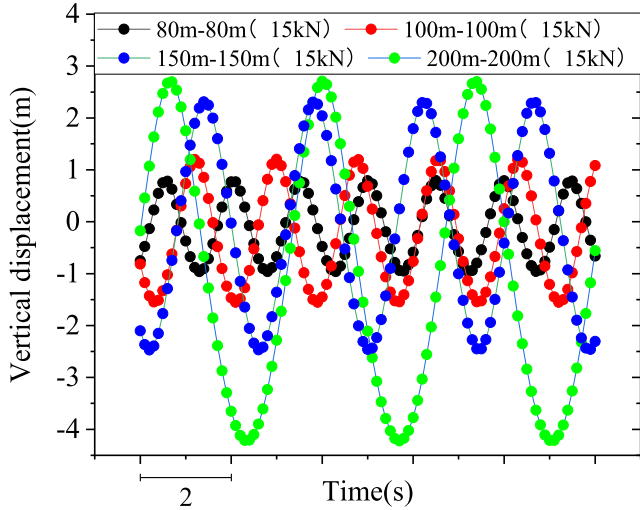
FIGURE 17. Displacement time-history curves of two-span transmission lines with equal span length (initial tension is 15 kN).
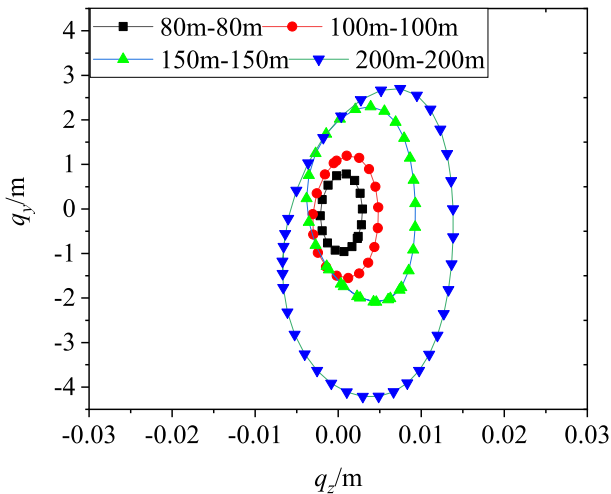

FIGURE 18. Galloping trace of two-span transmission lines with equal span length under different spans.

The modes drawn using theoretical Formula (9) are shown in Fig. 19.

Fig. 19 shows that the modal shapes of the two-span conductors with equal length are basically the same, and the increase in initial tension has little influence on the modal of the two-span conductors.

Different initial tensions span two displacement time history curves of the conductors, as shown in Fig. 19, and when the initial tension is 40 kN and above, the two conductors do not gallop because when the initial tension increases to more than 40 kN with a smaller sag, the damping ratio remains unchanged, causing the aerodynamic damping term to be positive and unable to absorb wind energy.

Fig. 20 shows that the time for the equal-span two-span conductors to gallop to stabilize gradually decreases with increasing initial tension. The amplitude of the two-span conductors with span lengths of 100 m-100 m (initial tension

TABLE 5. Frequency of two equal-span conductors at different initial tensions (length between 100 m -100 m).

Initial tension		20kN	30kN
Mode type	Calculation method	Frequency (Hz)	
First order in-plane symmetric mode frequency	Theoretical formula	0.550	0.673
	Abaqus	0.548	0.672
First order out-of-plane symmetric mode frequency	Theoretical formula	0.397	0.453
	Abaqus	0.393	0.442

20 kN) is 1.113 m, and that of the two-span conductors withspan lengths of 100 m-100 m (initial tension 30 kN) is 0.680 m. To more clearly compare the influence of the increase in initial tension on the opposite internal amplitude, the displacement time-history curves within 10 s are selected when the two conductors are galloping steadily, as shown in Fig. 21.

Fig. 21 shows that when the initial tension increases gradually, the amplitude of the equal-span two-span conductors decreases gradually, while when the initial tension is too large, the equal-span two-span conductors will not gallop. Compared with Fig. 8, as the initial tension increases from 15 kN to 20 kN, the amplitude of the two-span conductors decreases by 19.23%, while that of the single-span conductors increases by 12.32%. When the initial tension increases from 20 kN to 30 kN, the amplitude of the two-span conductors decreases by 38.90%, while that of the single-span conductors decreases by 177.69%.

The galloping traces of the two-span conductors with equal span lengths under different initial tensions are shown in Fig. 22.

Fig. 22 shows that when the initial tension increases, the galloping trace of the two-span conductors with lengths of 100 m to 100 m begins to decrease.

D. ANALYSIS OF GALLOPING CHARACTERISTICS OF THREE-SPAN CONDUCTORS
1) EFFECT OF SPAN LENGTH ON THE GALLOPING OF THREE-SPAN CONDUCTORS WITH UNEQUAL SPAN LENGTH

In this paper, when studying the influence of the change in adjacent span length on the overall galloping of the three-span conductors, the middle conductor length should be kept unchanged, and the conductor length on both sides should be consistent and gradually increased. Theoretical Equation (9) has the highest accuracy in calculating the in-plane frequency of the multispan conductors when the length between the spans is not equal. Therefore, this paper uses the theoretical formula to solve the in-plane frequency of the three-span conductors to avoid the same value. However, when using the theoretical Equation (14) to solve the out-of-plane frequency,
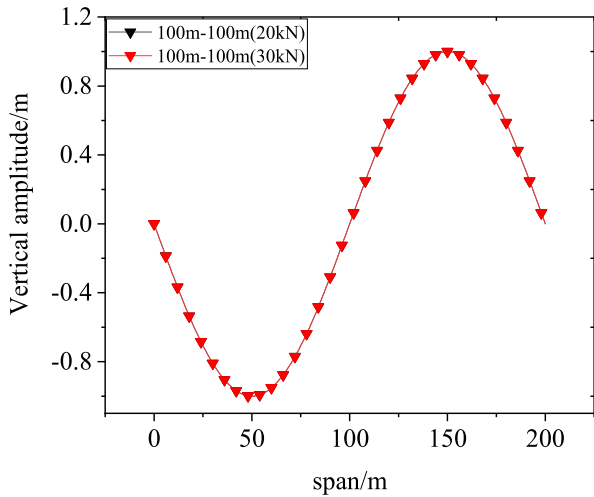
FIGURE 19. Mode diagram of two-span transmission lines with equal span length under different initial tensions.
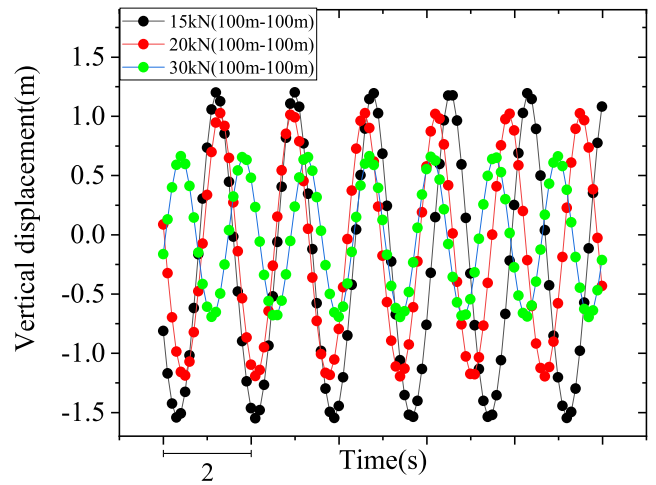

FIGURE 21. Displacement time-history curves of two equal-span transmission lines with equal span length (different initial tension).
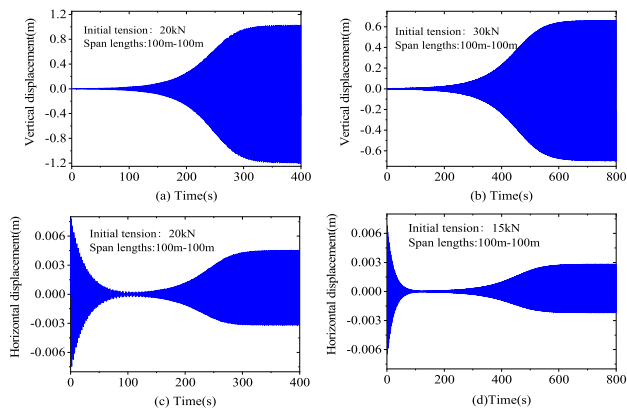

FIGURE 20. Displacement time-history curves of two-span transmission lines with equal span length (two-span length of 100 m -100 m).

FIGURE 22. Galloping trace of two-span transmission lines with equal span length under different initial tensions.

the value of the length between the spans can be directly substituted to ensure the highest accuracy. To verify the accuracy of the theoretical formula, Abaqus was used to establish the corresponding finite element model. The calculation results of the two algorithms are shown in Table 6.

Table 7 shows that the theoretical formula is close to the frequency calculated by Abaqus, so the frequency calculated by using the theoretical formula is accurate. The modes drawn using theoretical Equation (9) are shown in Fig. 23.

Fig. 23 shows that the modal shapes of the middle conductors are basically the same. As the length of the sub conductors on both sides increases at the same time, the amplitude of the conductor modes on both sides increases first and then decreases. Limited by space, this paper only gives the conductor modal diagram calculated by the finite element method when the length of the three-span conductors is 200 m- 100 m-200 m, as shown in Fig. 24.

Fig. 24 shows that the modal shapes obtained by Abaqus are basically consistent with Fig. 23, so the modes in Fig. 23 are also accurate.
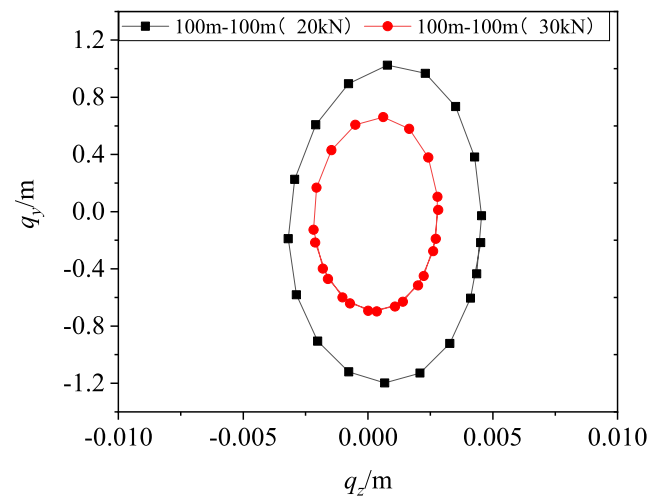
By substituting the frequency of the first-order mode in Table 6 into Equation (19), the displacement time-history curves of the three-span conductors are obtained, as shown in Fig. 25.

Fig. 25 shows that the time when the nonequal length three-span conductors gallops to stability gradually decreases with the simultaneous increase of the length of the two conductors on the edge. The amplitude of the three-span conductors with lengths of 50 m-100 m-50 m is 0.266 m, and that of the three-span conductors with lengths of 80 m-100 m-80 m is 0.904 m. The amplitude of the three-span conductors with a length of 150 m-100 m-150 m is 0.717 m, and that of the three-span conductors with a length of 200 m-100 m-200 m is 0.854 m. The multiscale method is used to calculate the amplitude of the three-span conductors with lengths of 200 m-100 m-200 m, which is 0.922. The results of the fourth-order Runge–Kutta method are basically consistent

TABLE 6. Frequency of nonequal pitch three-span conductors with an initial tension of 15 kN.

Span(m)		50 -100 -50	80 -100 -80	150 -100 -150	200 -100 -200
Mode type	Calculation method		Frequency (Hz)		
First order in-plane symmetric mode frequency	Theoretical formula	0.603	0.516	0.429	0.416
	Abaqus	0.601	0.515	0.430	0.417
First order out-of-plane symmetric mode frequency	Theoretical formula	0.344	0.331	0.275	0.221
	Abaqus	0.344	0.332	0.277	0.221
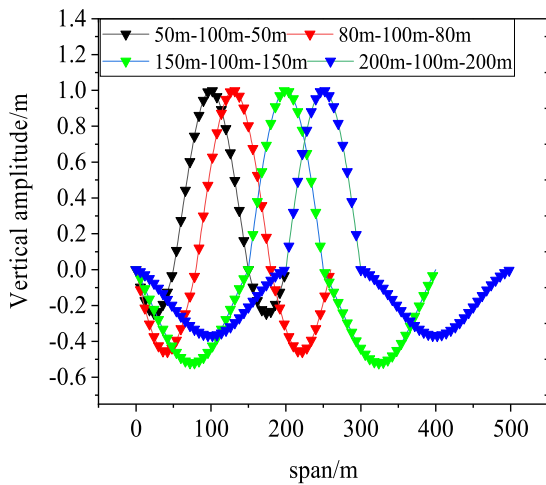
FIGURE 23. Mode diagram of three-span transmission lines with unequal span lengths.

FIGURE 24. Three-span conductor modes obtained by the finite element method.

with the multiscale method, proving that the three-span conductor model is also accurate.

To more clearly compare the influence of the increase in the length of adjacent spans on the amplitude of the nonequal-length three-span conductors, the displacement time-history curves of the three-span conductors within 10 s after it gallops steadily are shown in Fig. 26.

As shown in Fig. 26, when the length of the two conductors on the edge is smaller than the length of the middle conductors, the amplitude of the three-span conductors increases as the length of the two conductors on the edge increases at the same time. When the length of the two conductors on the edge is greater than the length of the middle conductors, the amplitude of the three-span conductors increases with increasing length of the two conductors on the edge.

The galloping traces of the three-span conductors with unequal span lengths are shown in Fig. 27.

Fig. 27 shows that the galloping traces of the three-span conductors with unequal span lengths are basically elliptical.

Because there are many conductors hanging on the tension tower at present, as shown in Fig. 28, if the conductor
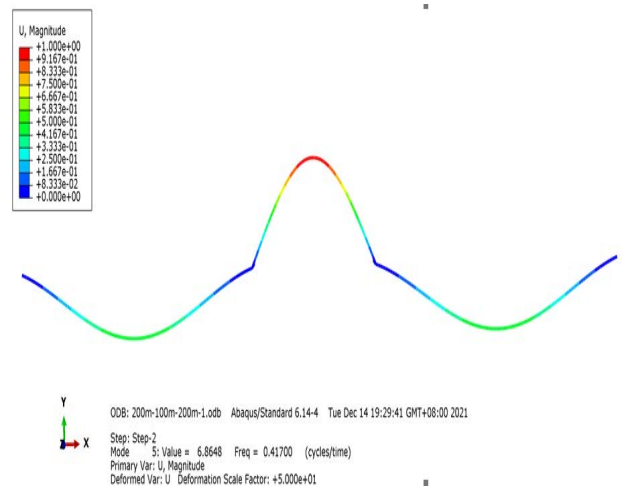
distance is too close, it will cause accidents such as interphase flashover. Studying the amplitude of conductors is helpful for the design of lines in actual projects and provides a reference for preventing and controlling the interphase flashover of conductors.

2) EFFECT OF SPAN LENGTH ON THE GALLOPING OF THREE-SPAN CONDUCTORS WITH EQUAL SPAN LENGTH

In this paper, the influence of the galloping characteristics of three-span conductors with the length of the conductors is studied. Four three-span conductors with a gradual increase in span length are selected, and their frequencies are shown in Table 7.

Table 7 shows that the frequency calculated by the theoretical formula is accurate. The model obtained using theoretical Equation (9) is shown in Fig. 29.

As shown in Fig. 29, when the three conductors are spaced relatively close, the modal shapes of the three conductors are basically the same. However, when the three conductors are spaced relatively far apart, two downward half waves will
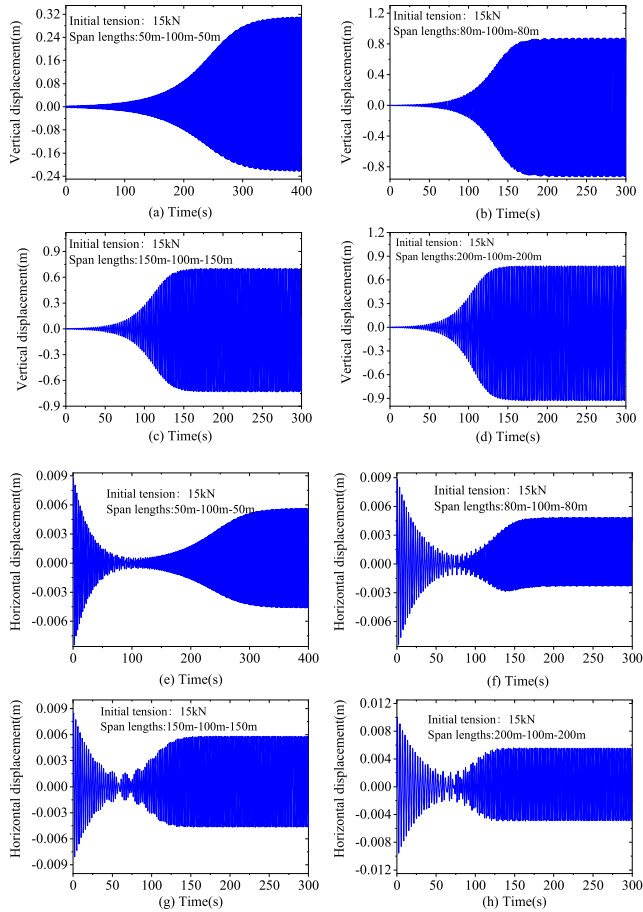
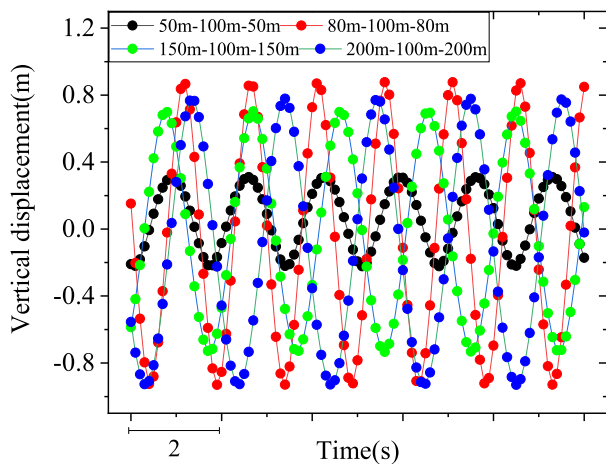**FIGURE 25.** Displacement time-history curves of three-span transmission lines with unequal span lengths.

FIGURE 26. Displacement time-history curves of three-span transmission lines with unequal span length (initial tension is 15 kN).

FIGURE 27. Galloping trace of three-span transmission lines with unequal span length under different spans.

FIGURE 28. Three-span transmission tower lines.

FIGURE 29. Mode diagram of three-span transmission lines with equal span length.

appear in each conductor. This is due to the increase in the spans, and the conductor sag is too large.

After the frequency is obtained, the time-history curves of the displacement of the three-span conductors with equal length are calculated by the fourth-order Runge–Kutta method, as shown in Fig. 30.
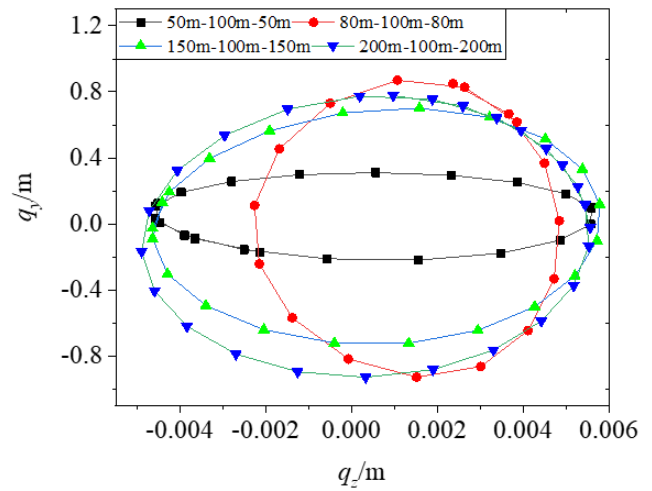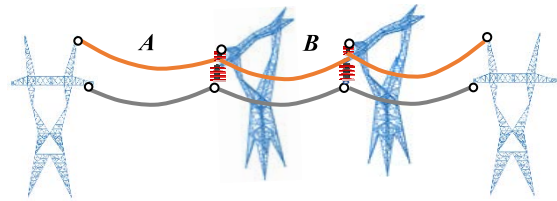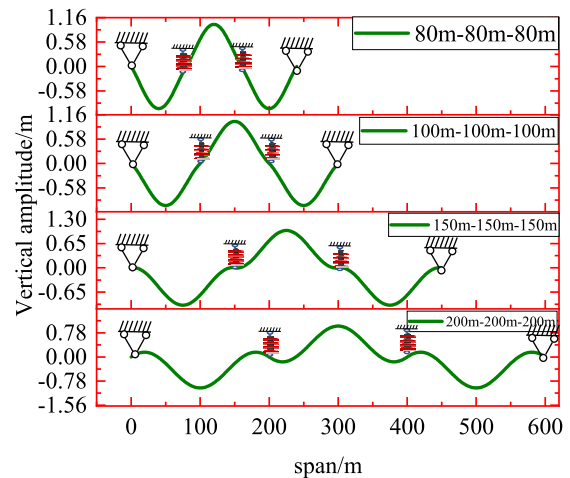
Fig. 30 shows that the galloping time of the equal-length three-span conductors tends to stabilize and gradually decrease with the simultaneous increase in the length of the three conductors. The amplitude of the three-span conductors with lengths of 80 m-80 m-80 m is 0.369 m, and that of the three-span conductors with lengths of 100 m-100 m-100 m is 0.413 m. Compared with (a), (b), (c) and (d) in Fig. 25, the amplitude of the three-span conductors is the minimum when the three conductor lengths are all equal. The amplitude of the

TABLE 7. Frequency of equal-pitch three-span conductors with an initial tension of 15 kN.

Span		80 m-80 m-80 m	100 m-100 m-100 m	150 m-150 m-150 m	200 m-200 m-200 m
Mode type	Calculation method		Frequency（Hz）		
First order in-plane symmetric mode frequency	Theoretical formula	0.589	0.472	0.315	0.237
	Abaqus	0.588	0.471	0.314	0.240
First order out-of-plane symmetric mode frequency	Theoretical formula	0.359	0.322	0.255	0.208
	Abaqus	0.357	0.323	0.257	0.209

three-span conductors with lengths of 150 m-150 m-150 m is 0.298 m, and that of the three-span conductors with lengths of 200 m-200 m-200 m is 0.454 m. The sudden drop in amplitude in Fig. 28 (a)-(c) is also because the in-plane frequency of the conductors is approximately twice the out-of-plane frequency when it gallops. To more clearly compare the influence of the amplitude of the third span conductors with the increase of the length between the secondary conductors and its counterpart, the displacement time-history curves of the three-span conductors within 10 s after it gallops steadily are shown in Fig. 31.

It can be seen from Fig. 31 shows that the amplitude of the three-span conductors with equal spacing increases first, then decreases, and then continues to increase.

The galloping traces of the three-span conductors with equal span lengths are shown in Fig. 32 below.

Fig. 32 shows that although the horizontal amplitudes in the figure seem to differ greatly, the actual horizontal amplitudes vary very little, and the galloping trace is mainly in the vertical direction.

3) EFFECT OF INITIAL TENSION ON THE GALLOPING OF THREE-SPAN CONDUCTORS WITH EQUAL SPAN LENGTH

In this paper, the influence of initial tension on the galloping characteristics of parallel and three-span conductors is studied. Two common initial tensions of transmission lines are selected, and their frequencies are shown in Table 8.

Table 7 shows that the frequency calculated by the theoretical formula is accurate. The model obtained using theoretical Equation (9) is shown in Fig. 33.

Fig. 33 shows that the shape of the three-span conductors is basically the same under two different initial tensions, and the initial tension has little influence on the modal shape of the three-span conductors.

After obtaining the frequency, the fourth-order Runge–Kutta method is used to calculate the time-history curves of the displacement of the three-span conductors with equal length under different initial tensions, as shown in Fig. 34.
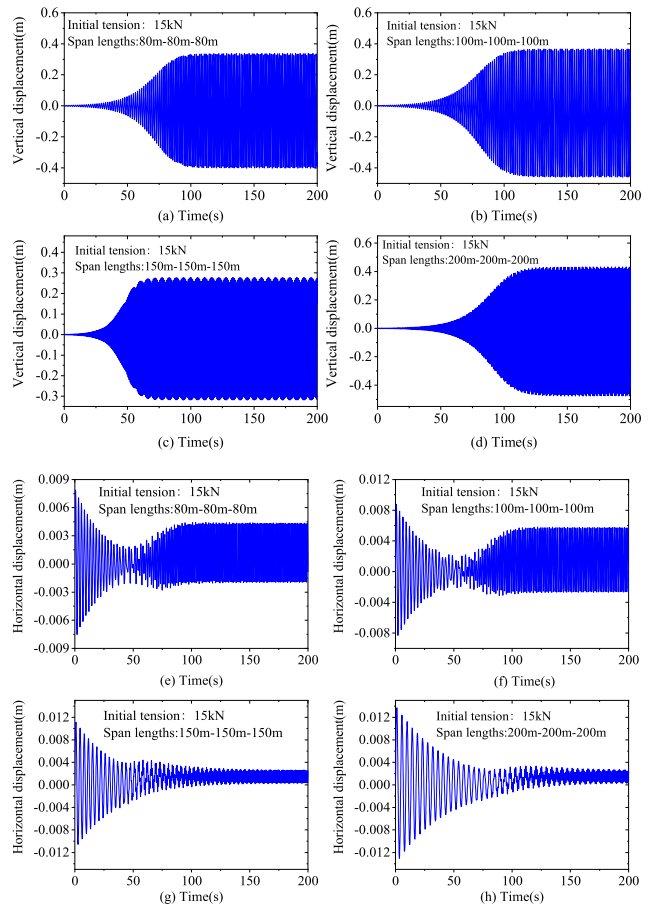
FIGURE 30. Displacement time-history curves of three-span transmission lines with unequal spans.

Fig. 34 shows that the galloping time of equal-span three-span conductors tends to stably decrease first and then increase with increasing initial tension. The amplitude of the three-span conductors with an initial tension of 20 kN (three-span length of 100 m-100 m-100 m) is 0.204 m. The amplitude of the three-span conductors with an initial tension of 30 kN (three-span length of 100 m-100 m-100 m) is
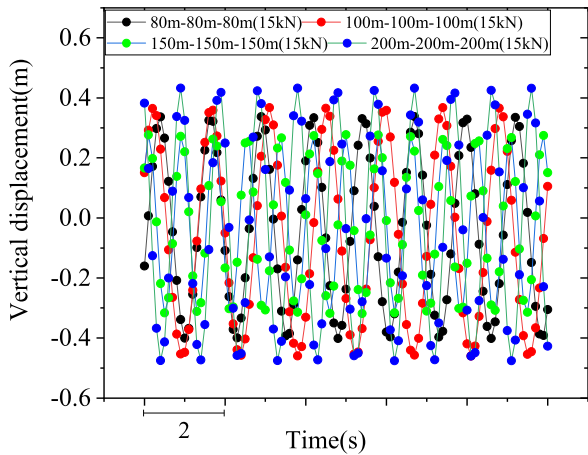
FIGURE 31. Displacement time-history curves of three-span transmission lines with equal span length (initial tension is 15 kN).

FIGURE 32. Galloping trace of three-span transmission lines with equal span length under different spans.

FIGURE 33. Mode diagram of three-span transmission lines with equal span length under different initial tensions.
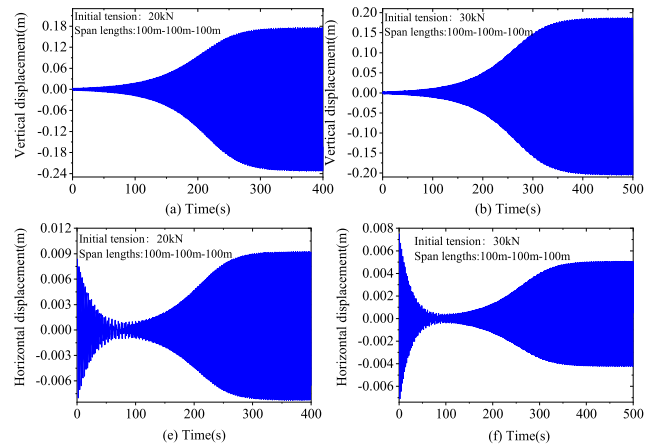

FIGURE 34. Displacement time-history curves of three-span transmission lines with equal span length (three-span length of 100 m -100 m -100 m).
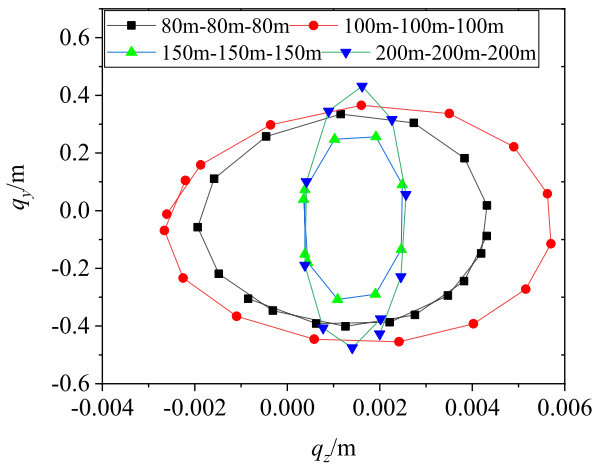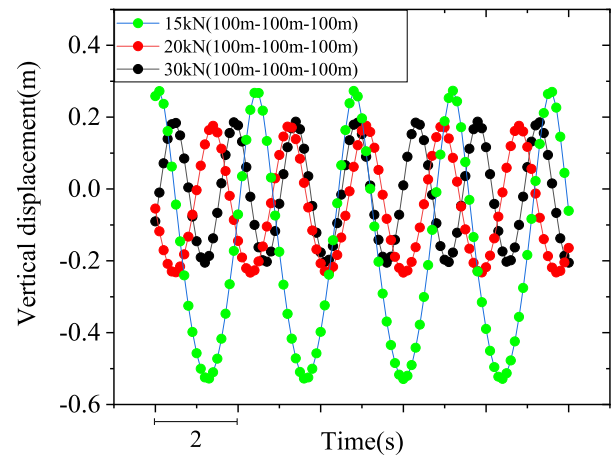

FIGURE 35. Displacement time-history curves of three-span transmission lines with equal span length (different initial tension).

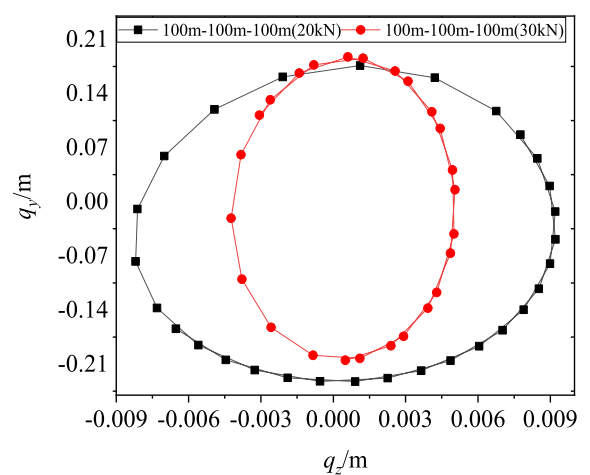**FIGURE 36.** Galloping trace of three-span transmission lines with equal span length under different initial tensions.

0.196 m. To more clearly compare the influence of the initial tension of the conductors on the increase of the amplitude, the

displacement time-history curves of the third-span conductors within 10 s after it gallops steadily are shown in Fig. 35.

TABLE 8. Frequency of three-span conductors with equal span length under different initial tensions (span length of 100 m-100 m-100 m).

Initial tension		20kN	30kN
Modal type	Calculation method	Frequency（Hz）	
First order in-plane symmetric mode frequency	Theoretical formula	0.545	0.668
	Abaqus	0.551	0.667
First order out-of-plane symmetric mode frequency	Theoretical formula	0.345	0.381
	Abaqus	0.345	0.377

Fig. 35 shows that when the initial tension increases, the amplitude of the equal-pitch three-span conductors increases first and then decreases. Compared with Fig. 21, as the initial tension increases from 15 kN to 20 kN, the amplitude of the three-span conductors decreases by 50.60%, and the two-span conductors decrease by 19.23%. When the initial tension increases from 20 kN to 30 kN, the amplitude of the three-span conductors decreases by 20.40%, while that of the two-span conductors decreases by 38.90%.

Therefore, when the initial tension increases, the amplitude of the single-span conductors first increases slowly and then decreases greatly, the amplitude of the equal-pitch two-span conductors first decreases slightly and then decreases greatly, and the amplitude of the equal-pitch three-span conductors first decreases significantly and then decreases slightly.

The galloping traces of the three-span conductors with equal span lengths under different initial tensions are shown in Fig. 36.

Fig. 36 shows that the galloping track of the three-span conductors with equal span length under different initial tensions decreases with increasing initial tension.

VII. CONCLUSION

In this paper, the influence of insulator strings and adjacent spans was taken into account when establishing the multispan conductor galloping model, and the galloping characteristics of multispan conductors under different parameters were analyzed when all the conductors in the whole tension section met the galloping conditions. The research results are as follows.

1) The amplitude of the multispan conductors is obviously greater than that of the single-span conductors, so the interaction between adjacent spans has a great influence on the galloping characteristics of ice-covered conductors. The galloping amplitude increases first and then decreases with increasing span number.

2) The galloping amplitude of the two-span conductors with nonequal spans increases with increasing length between adjacent conductors, and the galloping amplitude

of the two-span conductors with equal spans also increases with increasing length between each span of conductors. Keeping the span of the two-span conductors unequal reduces the amplitude. As the initial tension increases gradually, the galloping amplitude of the two-span conductors with equal spans decreases. When the initial tension is large enough, galloping will not occur.

3) The galloping amplitude of the three-span conductors with nonequal span or equal span increases first, then decreases and then continues to increase with the increase in the length between adjacent spans. Keeping the span of the three-span conductors consistent can reduce the amplitude. With increasing initial tension, the galloping amplitude of the three-span conductors with equal spans decreases.

APPENDIX

$$b_1 = \int_0^{l_i} m\psi_{yj}^2 dx, \, b_2 = \int_0^{l_i} \mu_2 \psi_{yj}^2 dx,$$

$$b_3 = \int_0^{l_i} (-y'' \frac{EA}{l_e} \sum_{i=1}^{N} \int_0^{l_i} y_i' \psi_{yi}' dx - H\psi_{yj}'') \psi_y dx,$$

$$b_4 = -\int_0^{l_i} \{ \frac{EA}{l_e} \psi_{yj}'' \sum_{i=1}^{N} \int_0^{l_i} y_i' \psi_{yji}' dx + y'' \frac{EA}{2l_e} \sum_{i=1}^{N} \int_0^{l_i} \psi_{yji}'^2 dx \} \psi_{yj} dx,$$

$$b_5 = -\int_0^{l_i} (\frac{EA}{2l_e} y'' \sum_{i=1}^{N} \int_0^{l_i} \psi_{zi}'^2 dx) \psi_{yj} dx,$$

$$b_6 = -\int_0^{l_i} (\frac{EA}{2l_e} \psi_{y''} \sum_{i=1}^{N} \int_0^{l_i} \psi_{yi}'^2 dx) \psi_y dx,$$

$$b_7 = -\int_0^{l_i} (\frac{EA}{2l_e} \psi_{y''} \sum_{i=1}^{N} \int_0^{l_i} \psi_{zi}'^2 dx) \psi_y dx,$$

$$pp_y = \int_0^{l_i} p_y \psi_y dx$$

$$c_1 = \int_0^{l_i} m\psi_z^2 dx, \, c_2 = \int_0^{l_i} \mu_z \psi_z^2 dx,$$

$$c_3 = \int_0^{l_i} (-H\psi_z'') \psi_z dx$$

$$c_4 = -\int_0^{l_i} (\frac{EA}{l_e} \psi_z'' \sum_{i=1}^{N} \int_0^{l_i} y_i' \psi_{yi}' dx) \psi_z dx,$$

$$c_5 = -\int_0^{l_i} (\frac{EA}{2l_e} \psi_z'' \sum_i^{N} \int_0^{l_i} \psi_{yi}'^2 dx) \psi_z dx$$

$$c_6 = -\int_0^{l_i} (\frac{EA}{2l_e} \psi_z'' \sum_{i=1}^{N} \int_0^{l_i} \psi_z'^2 dx) \psi_z dx,$$

$$pp_z = \int_0^{l_i} p_z \psi_z dx$$

$$d_1 = \int_0^{l_i} J\psi_\theta^2 dx, \, d_2 = \int_0^{l_i} \mu_\theta \psi_\theta^2 dx,$$

$$d_3 = \int_0^{l_i} (-GI_P\psi_\theta'')\psi_\theta dx$$

$$pp_\theta = \int_0^{l_i} p_\theta \psi_\theta dx$$

$$\bar{b}_2 = \int_0^{l_i} \mu_2\psi_y^2 + \frac{1}{2}\rho U^2 D(\frac{\lambda_1}{U})\psi_y^2 dx,$$

$$b_9 = -\int_0^{l_i} [\frac{1}{2}\rho U^2 D(\frac{\lambda_2}{U^2})\psi_y^2]\psi_y dx,$$

$$b_{10} = \int_0^{l_i} [\frac{1}{2}\rho U^2 D(\frac{\lambda_3}{U^3})\psi_y^3]\psi_y dx.$$

$$c_8 = \int_0^{l_i} [\frac{1}{2}\rho U^2 D(\frac{\lambda_4}{U})\psi_y]\psi_z dx,$$

$$c_9 = -\int_0^{l_i} [\frac{1}{2}\rho U^2 D(\frac{\lambda_5}{U^2})\psi_y^2]\psi_z dx$$

$$c_{10} = \int_0^{l_i} [\frac{1}{2}\rho U^2 D(\frac{\lambda_6}{U^3})\psi_y^3]\psi_z dx$$

$$d_4 = \int_0^{l_i} [\frac{1}{2}\rho U^2 D^2(\frac{\lambda_7}{U})\psi_y]\psi_\theta dx,$$

$$d_5 = -\int_0^{l_i} [\frac{1}{2}\rho U^2 D^2(\frac{\lambda_8}{U^2})\psi_y^2]\psi_\theta dx$$

$$d_6 = \int_0^{l_i} [\frac{1}{2}\rho U^2 D^2(\frac{\lambda_9}{U^3})\psi_y^3]\psi_\theta dx$$

$$\omega_2^2 = \frac{b_3}{b_1}, b_1' = \frac{\bar{b}_2}{b_1}, b_2' = \frac{b_4}{b_1}, b_3' = \frac{b_5}{b_1}, b_4' = \frac{b_6}{b_1},$$

$$b_5' = \frac{b_7}{b_1}, b_7' = \frac{b_9}{b_1}, b_8' = \frac{b_{10}}{b_1},$$

$$\omega_3^2 = \frac{c_3}{c_1}, c_1' = \frac{c_2}{c_1}, c_2' = \frac{c_4}{c_1}, c_3' = \frac{c_5}{c_1}, c_4' = \frac{c_6}{c_1},$$

$$c_6' = \frac{c_8}{c_1}, c_7' = \frac{c_9}{c_1}, c_8' = \frac{c_{10}}{c_1},$$

REFERENCES

[1] J. Chan, "Wind-induced condutor motion," in *EPRl Transmission Line Reference Book*, 2nd ed. Palo Alto, CA, USA: Electric Power Research Institute, 2009.

[2] J. P. D. Hartog, "Transmission line vibration due to sleet," *Trans. Amer. Inst. Electr. Eng.*, vol. 51, no. 4, pp. 1074–1076, Dec. 1932.

[3] O. Nigol and G. J. Clarke, "Conductor galloping and control based on torsional mechanism," *IEEE Trans. Power App. Syst.*, vol. PAS-93, no. 6, p. 1729, Feb. 1974.

[4] O. Nigol and P. Buchan, "Conductor galloping part i–den hartog mechanism," *IEEE Trans. Power App. Syst.*, vol. PAS-100, no. 2, pp. 699–707, Feb. 1981, doi: 10.1109/tpas.1981.316921.

[5] P. Yu, "Instability trends of inertially coupled galloping part II: Periodic vibrations," *J. Sound Vib.*, vol. 183, no. 4, pp. 679–691, Jun. 1995, doi: 10.1006/jsvi.1995.0179.

[6] P. Yu, A. H. Shah, and N. Popplewell, "Inertially coupled galloping of iced conductors," *J. Appl. Mech.*, vol. 59, no. 1, pp. 140–145, Mar. 1992, doi: 10.1115/1.2899419.

[7] Z. Wan, D. Zhang, Z. Li, S. Mo, and Y. Zhang, "A wind tunnel study on the aerodynamic characteristics of ice-accreted twin bundled conductors," *Int. J. Struct. Stability Dyn.*, vol. 22, no. 7, Jun. 2022, Art. no. 2250038, doi: 10.1142/s0219455422500389.

[8] O. Chabart and J. L. Lilien, "Galloping of electrical lines in wind tunnel facilities," *J. Wind Eng. Ind. Aerodynamics*, vols. 74–76, pp. 967–976, Apr. 1998, doi: 10.1016/s0167-6105(98)00088-9.

[9] J. Chadha and W. Jaster, "Influence of turbulence on the galloping instability of iced conductors," *IEEE Trans. Power App. Syst.*, vol. PAS-94, no. 5, pp. 1489–1499, Sep. 1975, doi: 10.1109/t-pas.1975.31991.

[10] X. Liu, B. Yan, and H. Zhang, "Numerical simulation for galloping of iced covered quad-bundled conductor under stochastic wind load," in *Proc. Asia–Pacific Power Energy Eng. Conf.*, 2010, pp. 1–4.

[11] H. M. Irvine and T. K. Caughey, "The linear theory of free vibrations of a suspended cable," *Proc. Roy. Soc. London Math. Phys. Sci.*, vol. 341, no. 1626, pp. 299–315, Dec. 1974, doi: 10.1098/rspa.1974.0189.

[12] H. M. Irvine, "Free vibrations of inclined cables," *J. Struct. Division*, vol. 104, no. 2, pp. 343–347, Feb. 1978, doi: 10.1061/jsdeag.0004860.

[13] Q. Wu, K. Takahashi, and S. Nakamura, "Formulae for frequencies and modes of in-plane vibrations of small-sag inclined cables," *J. Sound Vib.*, vol. 279, nos. 3–5, pp. 1155–1169, Jan. 2005, doi: 10.1016/j.jsv.2004.01.004.

[14] Y. M. Desai, P. Yu, N. Popplewell, and A. H. Shah, "Finite element modelling of transmission line galloping," *Comput. Struct.*, vol. 57, no. 3, pp. 407–420, Nov. 1995, doi: 10.1016/0045-7949(94)00630-l.

[15] P. Yu, Y. M. Desai, and N. Popplewell, "Three-degree-of-freedom model for galloping (Parts I and II)," *J. Eng. Mech.*, vol. 119, pp. 2405–2448, Dec. 1993, doi: 10.1061/(ASCE)0733-9399(1993)119:12(2426).

[16] S. W. Rienstra, "Nonlinear free vibrations of coupled spans of overhead transmission lines," *J. Eng. Math.*, vol. 53, nos. 3–4, pp. 337–348, Dec. 2005, doi: 10.1007/s10665-005-9011-4.

[17] X. Xie, X. Hu, J. Peng, and Z. Wang, "Refined modeling and free vibration of two-span suspended transmission lines," *Acta Mechanica*, vol. 228, no. 2, pp. 673–681, Feb. 2017, doi: 10.1007/s00707-016-1730-2.

[18] X. Liu, L. Liu, M. Cai, and B. Yan, "Free vibration of transmission lines with multiple insulator strings using refined models," *Appl. Math. Model.*, vol. 67, pp. 252–282, Mar. 2019, doi: 10.1016/j.apm.2018.10.021.

[19] J. Hu, B. Yan, S. Zhou, and H. Zhang, "Numerical investigation on galloping of iced quad bundle conductors," *IEEE Trans. Power Del.*, vol. 27, no. 2, pp. 784–792, Apr. 2012, doi: 10.1109/tpwrd.2012.2185252.

[20] H. Matsumiya, T. Nishihara, and T. Yagi, "Aerodynamic modeling for large-amplitude galloping of four-bundled conductors," *J. Fluids Struct.*, vol. 82, pp. 559–576, Oct. 2018, doi: 10.1016/j.jfluidstructs.2018.08.003.

[21] Z. Yan, Y. Zhu, Y. You, and J. Wang, "The response and instability of cross-rope suspension towers under harmonic excitation," *Int. J. Struct. Stability Dyn.*, vol. 17, no. 10, Nov. 2017, Art. no. 1750124, doi: 10.1142/s0219455417501243.

[22] X. Liu, S. Yang, G. Min, M. Cai, C. Wu, and Y. Jiang, "Investigation on the accuracy of approximate solutions obtained by perturbation method for galloping equation of iced transmission lines," *Math. Problems Eng.*, vol. 2021, pp. 1–18, Mar. 2021, doi: 10.1155/2021/6651629.

[23] A. T. Edwards and A. Madeyski, "Progress report on the investigation of galloping of transmission line conductors [includes discussion]," *Trans. Amer. Inst. Electr. Eng. III, Power App. Syst.*, vol. 75, no. 3, pp. 666–686, Jan. 1956, doi: 10.1109/AIEEPAS.1956.4499353.

[24] O. Barry, J. Zu, and D. Oguamanam, "Analytical and experimental investigation of overhead transmission line vibration," *J. Vib. Control*, vol. 21, no. 14, pp. 2825–2837, Jan. 2014, doi: 10.1177/1077546313517589.

[25] X.-H. Liu, B. Yan, H.-Y. Zhang, and S. Zhou, "Nonlinear numerical simulation method for galloping of iced conductor," *Appl. Math. Mech.*, vol. 30, no. 4, pp. 489–501, Apr. 2009, doi: 10.1007/s10483-009-0409-x.

[26] F. Benedettini, G. Rega, and F. Vestroni, "Modal coupling in the free nonplanar finite motion of an elastic cable," *Meccanica*, vol. 21, no. 1, pp. 38–46, Mar. 1986, doi: 10.1007/bf01556315.

[27] G. S. Byun and R. I. Egbert, "Two-degree-of-freedom analysis of power line galloping by describing function methods," *Electr. Power Syst. Res.*, vol. 21, no. 3, pp. 187–193, Jul. 1991, doi: 10.1016/0378-7796(91)90044-n.

JIA-YAN ZHENG was born in Suining, Sichuan, China, in 1976. She received the B.S. and M.S. degrees in mechanical engineering from Chongqing University, Chongqing, China, in 2000 and 2006, respectively. She is currently pursuing the Ph.D. degree in bridge engineering with Chongqing Jiaotong University, Chongqing. From 2000 to 2008, she was a Lecturer with Southwest University and a Lecturer with Chongqing Jiaotong University, from 2008 to 2011, where she has been an Associate Professor with Chongqing Jiaotong University, since 2011. Her research interests include machine-vision based bridge monitoring theory, high altitude road tunnel thermal protection and safety techniques, numerical simulation of high voltage wire, and insulator string system nonlinear vibration response/behavior under complex air pressure.

Her awards and honors include the Xuzhilun Outstanding Teacher Award from the Chinese Society of Theoretical and Applied Mechanics (CSTAM), in 2019, and the Huaxiluhang Outstanding Teacher Award from Chongqing Jiaotong University, in 2021.

XIAO-HUI LIU was born in Inner Mongolia, China, in 1981. He received the Ph.D. degree in engineering from Chongqing University, Chongqing, China, in 2011. He joined the College of Civil Engineering, Chongqing Jiaotong University, in 2011, and is currently an Associate Professor with the College of Civil Engineering. His research interest includes structural dynamics analysis of transmission lines.

• • •

QI-HANG SHEN was born in Sunzhou, Jiangsu, China, in 1997. He received the B.S. degree in civil engineering from the College of Suqian, Jiangsu, in 2019. He is currently pursuing the M.S. degree in bridge engineering with Chongqing Jiaotong University, Chongqing, China. His research interest includes structural dynamics analysis of transmission lines.